Calculations of Electrostatic Energies in Photosynthetic Reaction Centers†

Rhett G. Alden,‡ William W. Parson,*,‡ Zhen Tao Chu,§ and Arieh Warshel*,§

Contribution from the Department of Biochemistry, University of Washington, Seattle, Washington 98195, and Department of Chemistry, University of Southern California, Los Angeles, California 90007

Received December 21, 1994®

Abstract: The free energies of radical-pair states of photosynthetic bacterial reaction centers are examined by calculations based on the crystal structure of the reaction center from *Rhodopseudomonas viridis*. The calculations focus on the energies of the states P^+B^-H and P^+BH^-, where P is a bacteriochlorophyll dimer that serves as an electron donor in the photochemical electron-transfer reaction, H is the bacteriopheophytin that accepts the electron, and B is a bacteriochlorophyll that may act as an intermediary. Dielectric effects are treated microscopically by evaluating the induced dipoles on the protein atoms and on a grid of points representing the surrounding membrane and solvent. Calculations using both the crystallographic coordinates for the protein atoms and molecular-dynamics/free-energy-perturbation simulations are carried out with various treatments of the ionizable amino acid residues and with several different models of the membrane. Effects of electrolytes in the solvent are included. The dependence of the results on the size of the protein region that is treated explicitly in the model is examined. Calculations that do not include the membrane or solvent are shown to give unstable results that cannot be used to draw conclusions about the energies of the radical-pair states. On the other hand, accounting properly for the dielectric effects of the protein, membrane, and solvent makes the calculated free energies relatively insensitive to the size of the protein model, the charges assigned to the ionizable amino acid residues, and other details of the treatment. The calculations place P^+BH^- 6−7 kcal/mol below the excited singlet state of P, in good agreement with experimental measurements, and put P^+B^-H about 3 kcal/mol above P^+BH^- with an uncertainty of several kilocalories per mole. These results are consistent with the formation of P^+B^-H as an intermediate in the charge-separation reaction, although we cannot exclude the possibility that the reaction proceeds by a superexchange mechanism. Most of the ionized amino acid residues probably are sufficiently well screened so that they have only minor electrostatic effects on the energies of the relaxed P^+B^-H and P^+BH^- states, but the effects of two arginines and an aspartic acid residue could be significant. Fields from other ionized groups could be important on time scales that are short relative to relaxation of the protein and solvent dipoles. If the solvent is assigned a low polarity in order to model a long dielectric relaxation time, the calculated reorganization energies of the electron-transfer reactions are decreased but our conclusions about the energetics of the radical-pair states are not changed significantly.

The initial electron-transfer reaction in photosynthetic bacterial reaction centers is the transfer of an electron from the excited state (P*) of a reactive bacteriochlorophyll dimer (P) to a bacteriopheophytin (H), generating a P^+H^- radical pair. Despite major progress in structural and kinetic studies,[1,2] the mechanism of the reaction is still not well understood. In particular, it is not clear whether the reaction proceeds through an intermediate state (P^+B^-) in which an electron resides transiently on a bacteriochlorophyll molecule (B) that is located between P and H. An understanding of the role of B in the reaction hinges largely on the energy of P^+B^-, which cannot presently be measured experimentally. If P^+B^- lies substantially above P* in energy, it is unlikely to be formed as a real intermediate, in light of the observation that the charge-separation reaction occurs rapidly at cryogenic temperatures. P^+B^- could still play a role in coupling P* with P^+H^- electronically by superexchange, but the strength of the coupling also would diminish as the gap between P^+B^- widened. Theoretical evaluations of the energy of P^+B^- could contribute to an understanding of the reaction mechanism, provided that the calculations are reliable and are based on a sufficiently realistic model.

Early calculations by Creighton et al.[3a] and Parson et al.[3b] indicated that P^+B^- probably is located within about 3 kcal/mol of P*. Later work by Marchi et al.[4] gave a very different picture, in which P^+B^- lies about 20 kcal/mol above P*. What accounts for the large difference between these results? Al-

† Abbreviations: BChl, bacteriochlorophyll; BPh, bacteriopheophytin; FEP, free energy perturbation; LRF, local reaction field; MD, molecular dynamics; PDLD, protein dipole−Langevin dipole; SCAAS, self-consistent all-atoms solvent.

‡ University of Washington.

§ University of Southern California.

® Abstract published in *Advance ACS Abstracts,* November 15, 1995.

(1) (a) Deisenhofer, J.; Michel, H. *Science* **1989**, *245*, 1463−1473. (b) Allen, J. P.; Feher, G.; Yeates, T. O.; Komiya, H.; Rees, D. C. *Proc. Natl. Acad. Sci. U.S.A.* **1987**, *84*, 6162−6166. (c) El-Kabbani, O.; Chang, C.-H.; Tiede, D.; Norris, J.; Schiffer, M. *Biochemistry* **1991**, *30*, 5361−5369.

(2) (a) Michel-Beyerle, M. E., Ed. *Reaction Centers of Photosynthetic Bacteria*; Springer-Verlag: New York, 1990; 469 pp. (b) Breton, J., Verméglio, A., Eds. *The Photosynthetic Bacterial Reaction Center. II. Structure, Spectroscopy and Dynamics;* Plenum Press: New York, 1992; 429 pp. (c) Deisenhofer, J., Norris, J. R., Eds. *The Photosynthetic Reaction Center;* Academic Press: New York, 1993; Vol. I, 432 pp. (d) Deisenhofer, J., Norris, J. R., Eds. *The Photosynthetic Reaction Center;* Academic Press: New York, 1993; Vol. II, 574 pp.

(3) (a) Creighton, S.; Hwang, J.-K.; Warshel, A.; Parson, W. W.; Norris, J. *Biochemistry* **1988**, *27*, 774−781. (b) Parson, W. W.; Chu, Z. T.; Warshel, A. *Biochim. Biophys. Acta* **1990**, *1017*, 251−272. (c) Warshel, A.; Chu, Z. T.; Parson, W. W. *J. Photochem. Photobiol., A* **1994**, *82*, 123−128. (d) Parson, W. W.; Warshel, A. In *Anoxygenic Photosynthetic Bacteria*; Blankenship, R. E., Madigan, M. T., Bauer, C. E., Eds.; Kluyer Academic Publishers: Amsterdam, 1994; pp 559−575. (e) Alden, R. G.; Parson, W. W.; Chu, Z. T.; Warshel, A. In *Reaction Centers of Photosynthetic Bacteria. Structure and Dynamics*; Michel-Beyerle, M. E., Ed.; Springer-Verlag: Berlin, 1995; in press.

(4) Marchi, M.; Gehlen, J. N.; Chandler, D.; Newton, M. J. *J. Am. Chem. Soc.* **1993**, *115*, 4178−4190.

0002-7863/95/1517-12284$09.00/0

though the approaches used have some features in common, they differ in a number of respects. Marchi et al. included the entire protein structure in their computer model, whereas Parson et al. trimmed the protein to a smaller region around the electron carriers. Marchi et al. included the crystallographic water molecules, but neglected the mobile solvent molecules in and around the protein; Creighton et al. and Parson et al. included only a few of the X-ray waters but embedded the protein either in explicit water molecules or in a grid of polarizable atoms intended to simulate the surrounding membrane and water. Marchi et al. assumed that all the potentially ionizable amino acid residues were in their ionized forms; Creighton et al. and Parson et al. employed a thermodynamic cycle that started by taking these residues to be uncharged and then used a macroscopic model to evaluate the possible effects of charging those residues located within about 20 Å of the electron carriers. Parson et al. considered induced dipoles in the protein and the surrounding material explicitly; Marchi et al. used a homogeneous dielectric constant to represent the screening of electrostatic interactions of the pigments with the protein atoms, but did not consider the self-energies of the oxidized and reduced electron carriers. Finally, Marchi et al. used molecular orbital calculations to estimate the energies for transferring an electron from P to B or H in a vacuum, whereas Creighton et al. and Parson et al. used measured redox potentials in combination with calculated solvation energies. The consequences of some of these differences have been discussed recently elsewhere.[3c-e]

Here we reexamine the electrostatic energies of P^+B^- and P^+H^- and consider some of the difficulties in calculating electrostatic energies in proteins. We show that when the dielectric effects of the membrane and solvent that surround and penetrate the protein are considered, the calculations can lead to stable results for models with radii as small as 20 Å. The calculated energy difference between P^+B^- and P^+H^- is relatively insensitive to variations in the model, but does depend on the charges assigned to several of the ionizable amino acid residues. The present simulations agree with those of Creighton et al.[3a] and Parson et al.[3b] in placing P^+B^- close to P* in energy. They appear to be consistent with the formation of P^+B^- as an intermediate in the electron-transfer reaction, although, as we have noted previously,[3a] the uncertainties in such calculations are too large to exclude the superexchange mechanism unambiguously. The disagreement between our conclusions and those of Marchi et al.[4] can be attributed mainly to Marchi et al.'s neglect of the self-energies of the electron carriers and of the screening of ionized side chains by the surrounding solvent.

Methods

Consider the free energy change associated with transferring an electron from B^- to H in the presence of P^+. If we label PBH, P*BH, P^+B^-H, and P^+BH^- as states 0, 1, 2, and 3, respectively, the standard free energy change for this reaction can be expressed as

$$\Delta G_{23}^\circ = \Delta E^{gas} + \Delta V_{QQ} + \Delta G_{sol}^{pro} \qquad (1)$$

Here ΔE^{gas} is the energy change for the reaction $B^- + H \rightarrow B + H^-$ when the BChl and BPh molecules are separated at infinite distance in a vacuum, ΔV_{QQ} is the change in the energy of the direct interactions between B and H for the same reaction when the electron carriers are at their actual positions in the protein (but still *in vacuo*), and ΔG_{sol}^{pro} represents the change in the interaction of the electron carriers with the protein and the surrounding medium. Since the excitation energy of P (ΔG_{01}°) is known and the free energy difference between P*BH and P^+BH^- (ΔG_{13}°) can be measured experimentally,[5] an accurate calculation of ΔG_{23}° should determine the location of P^+B^-H.

In principle, ΔE^{gas} can be obtained by quantum mechanical calculations.[4,6] However, such calculations are not yet able to give accurate ionization energies and electron affinities for such large molecular systems as B and H. It therefore seems more reliable to make use of experimental information on the midpoint redox potentials of B and H or of bacteriochlorophyll (BChl) and bacteriopheophytin (BPh) in solution.[3] This can be done by using

$$\Delta E^{gas} = -\mathcal{F}[E_m^H - E_m^B] - \Delta G_{sol}^{ref} \qquad (2)$$

Here $\mathcal{F}$ is the Faraday constant, E_m^B and E_m^H are the measured midpoint potentials of the $BChl/BChl^-$ and BPh/BPh^- couples, and ΔG_{sol}^{ref} is the difference between the changes in solvation energy for the reactions $BPh + e^- \rightarrow BPh^-$ and $BChl + e^- \rightarrow BChl^-$ under the reference conditions of the redox measurements. Figure 1 shows these relationships in the form of a thermodynamic cycle.

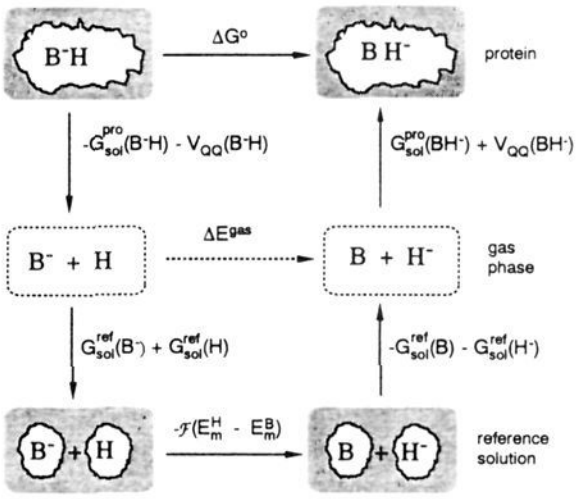

Figure 1. Thermodynamic cycle showing how the standard free energy change for the reaction $P^+B^-H \rightarrow P^+BH^-$ (ΔG°) can be obtained by combining the midpoint redox potentials of B and H (E_m^B and E_m^H) with the solvation energies of the electron carriers in the protein and in reference solutions. The states at the top of the drawing represent the electron carriers in the protein, those in the middle the carriers after separation at inifinite distance in a gas phase, and those at the bottom the separated carriers in the solutions used for the redox titrations. Transferring the electron carriers from the protein to the gas phase involves loss of the energy of direct interaction of the electron carriers (V_{QQ}), in addition to loss of G_{sol}^{pro}. The path through the reference states circumvents a quantum mechanical calculation of the gas-phase energy difference (ΔE^{gas}). The change in solvation energy in the protein is $\Delta G_{sol}^{pro} = G_{sol}^{pro}(BH^-) - G_{sol}^{pro}(B^-H)$, and that in the reference reaction is $\Delta G_{sol}^{ref} = G_{sol}^{ref}(H^-) - G_{sol}^{ref}(H) + G_{sol}^{ref}(B) - G_{sol}^{ref}(B^-)$. The change in direct interactions between B and H is $\Delta V_{QQ} = V_{QQ}(BH^-) - V_{QQ}(B^-H)$. The vertical positions of the states are schematic and do not represent the relative energies.

Equation 2 circumvents a quantum mechanical calculation of the gas-phase energies. In addition, eqs 1 and 2 reduce the calculation of ΔG_{23}° largely to an evaluation of the difference between the changes in solvation energies for the electron carriers in the reaction center (ΔG_{sol}^{pro}) and in solution (ΔG_{sol}^{ref}). This is advantageous because some types of errors and model dependencies tend to cancel out in the result.

Given the molecular structure and the partial charges on the atoms of B, B^-, H, and H^-, ΔV_{QQ} can be obtained by summing the charge−charge interaction energies, using a dielectric constant of 1. (We neglect the weak resonance interactions between B and H.) Evaluation of the solvation energies is more problematic. Apart from macroscopic, reaction-field treatments that would not be very useful in the case at hand, the three main alternatives are the protein-dipole−Langevin-dipole

(5) (a) Woodbury, N. W. T.; Parson, W. W. *Biochim. Biophys. Acta* **1984**, *767*, 345−361. (b) Chidsey, C. E. D.; Takif, L.; Boxer, S. G. *Proc. Natl. Acad. Sci. U.S.A.* **1985**, *82*, 6850−6854. (c) Hörber, J. K. H.; Göbel, W.; Ogrodnik, A.; Michel-Beyerle, M. E.; Cogdel, R. J. *FEBS Lett.* **1986**, *198*, 273−278. (d) Williams, J. C.; Alden, R. G.; Murchison, H. A.; Peloquin, J. M.; Woodbury, N. W.; Allen, J. P. *Biochemistry* **1992**, *31*, 11029−11037. (e) Woodbury, N. W. T.; Parson, W. W.; Gunner, M. R.; Prince, R. C.; Dutton, P. L. *Biochim. Biophys. Acta* **1986**, 851, 6−22.

(6) (a) Scherer, P. O. J.; Fischer, S. F. *Chem. Phys.* **1989**, *131*, 115−127. (b) Thompson, M. A.; Zerner, M. C. *J. Am. Chem. Soc.* **1991**, *113*, 8210−8215.

(PDLD) approach,[3b,7-9] free-energy-perturbation (FEP) calculations using molecular-dynamics (MD) simulations with an all-atom model,[3ac,4,9,10] and discretized-continuum (Poisson–Boltzmann) models.[10b,11] In the present work we employed both a modified PDLD approach and FEP/MD simulations.

PDLD Approach. In this approach, the change in solvation energy is written as

$$\Delta G_{sol} = \Delta V_{Q\mu} + \Delta V_{ind} + \Delta V_{H_2O} + \Delta V_{memb} + \Delta V_{ions} + \Delta V_{bulk} \quad (3)$$

Here $\Delta V_{Q\mu}$ is the change in the energy of direct electrostatic interactions of B and H with the charges of the atoms seen in the X-ray structure, *i.e.*, the protein, crystallographic water molecules, P^+, and electron carriers other than B and H themselves. ΔV_{ind} represents interactions of B and H with induced dipoles in the atoms of the X-ray structure, again excluding B and H themselves, ΔV_{H_2O} interactions with mobile solvent molecules that are not resolved in the crystal structure, ΔV_{memb} interactions with detergents or membrane phospholipids, ΔV_{ions} interactions with electrolytes in the solvent or the polar region of the membrane, and ΔV_{bulk} interactions with bulk solvent outside the region of the structure that is treated microscopically. The direct electrostatic interactions ($\Delta V_{Q\mu}$ and ΔV_{ions}) are evaluated using a dielectric constant of 1; ΔV_{ind}, ΔV_{H_2O}, and ΔV_{memb} are evaluated by iterative procedures that seek self-consistent solutions for the induced dipoles in the pigments and protein and on a grid of points surrounding the protein. In the present calculations, interactions of P and B with their histidine axial ligands were included in $\Delta V_{Q\mu}$.

All of the calculations began with the molecular structure of the *Rhodopseudomonas viridis* reaction center[1a] (Figure 2A), to which hydrogen atoms were added on the basis of idealized bonding geometries. The dihydroneurosporene, BChl, BPh, quinone, heme, and water molecules of the X-ray structure were included, but not the lauryldimethylamine oxide, octylglucoside, and sulfates. The hydrogens of all serine, threonine and tyrosine –OH groups, the $-CO_2H$ group of Glu(L)104, and the crystallographic water molecules were rotated into favorable orientations by a Metropolis Monte Carlo method. Starting with all the hydrogen atoms in default orientations, a particular rotatable hydrogen was chosen at random, and a torsional rotation was attempted by a randomly chosen angle. A measure of the change in the energy of the system, ΔU, was obtained by evaluating the van der Waals and charge–charge interactions of the hydrogen with the other atoms of the protein, pigments, and crystallographic water molecules. For a rotation of atom i,

$$U = \sum_{j \neq i} (A_j r_{ij}^{-12} + B_j r_{ij}^{-6} + C q_i q_j r_{ij}^{-1} d_{ij}^{-1}) \quad (4)$$

where the summation runs over all the atoms that are not bonded to i, r_{ij} is the distance between atoms i and j, the van der Waals coefficients A_j and B_j and atomic charges q_i and q_j are taken from the ENZYMIX[9a] force field, $C = 332$ kcal·mol^{-1}·Å·e^{-2}, and d_{ij} is a dielectric screening factor that we set equal to r_{ij}. The values of U given by eq 4 are not intended to be estimates of the actual energy of the system; they merely provide a tool for finding the most likely positions of the hydrogens. If the calculated ΔU was negative, the rotation was accepted; if ΔU was positive, the rotation was accepted with probability $\sigma = \exp(-\Delta U/k_B T)$, where k_B and T are the Boltzmann constant and temperature, and rejected with probability $1 - \sigma$. This procedure was continued for 10^5 iterations at a temperature of 1000 K, and for an additional 4×10^5 iterations as T was reduced gradually to 100 K. For these preliminary equilibrations, the structures included all the amino acid residues, pigments, and crystallographic water molecules within 40 Å

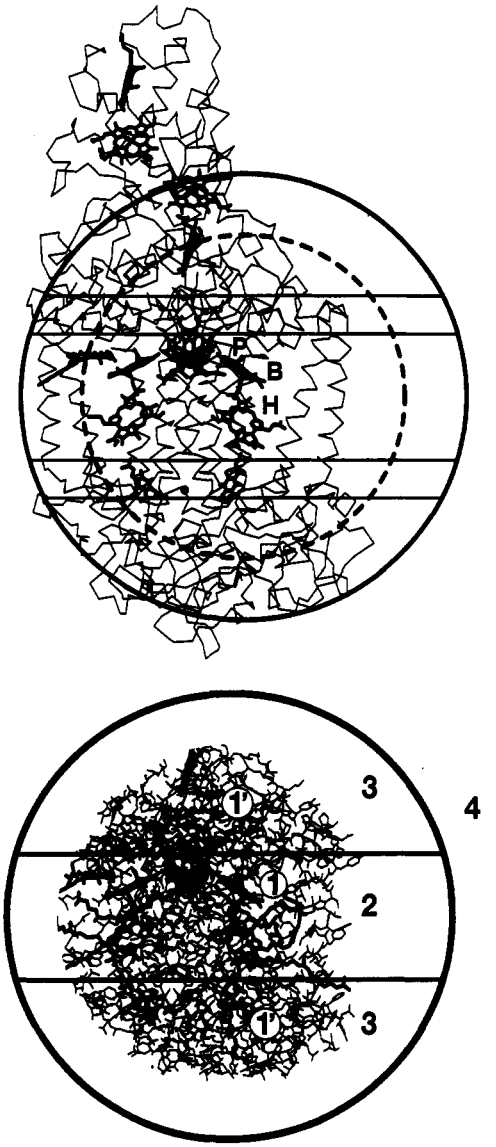

Figure 2. (A, top) Pigments and α-carbon backbone of the *Rp. viridis* reaction center. The bacteriochlorophyll dimer (P), the bacteriopheophytin that undergoes photoreduction (H), and the BChl that may be an intermediate electron carrier (B) are labeled. The unlabeled pigments include a carotenoid and additional molecules of BChl and BPh that do not participate in the normal charge-separation reactions (left side of the drawing), two quinones that serve as secondary electron acceptors (bottom), and four hemes that are secondary electron donors (top). The models of the protein for the PDLD-type calculations included all atoms within a sphere centered midway between B and H, along with the atoms of functional groups that extended across the boundary; the dashed circle in (A) shows the radius of 32 Å that was used in most of the calculations. (B, bottom) Protein and pigments after trimming to a sphere of 32 Å. In both (A) and (B), the solid circle (radius $b = R_{grid} + s_{grid}/2 = 43.5$ Å) indicates the outer limit of the grid of induced dipoles used to represent the solvent and membrane surrounding the protein. The horizontal lines indicate possible boundaries for the nonpolar region of the membrane; separate calculations were carried out with models in which this region had a thickness of either 25 Å (pair of lines in (B) and inner pair of lines in (A)) or 40 Å (outer pair of lines in (A)). Various atomic polarizabilities were assigned to grid points in the regions labeled 1, 1′, 2, and 3 in (B) (see text). The solvent outside the grid region (B, region 4) was treated as a continuum. The calculations included hydrogen atoms (not shown), the phytyl side chains of the BChls and BPhs, and the prenyl tails of the quinones (truncated in (A) for clarity).

(7) (a) Warshel, A.; Russell, S. T. *Q. Rev. Biophys.* **1984**, *17*, 283–422. (b) Russell, S. T.; Warshel, A. *J. Mol. Biol.* **1985**, *185*, 389–404. (c) Warshel, A.; Aqvist, J. *Annu. Rev. Biophys. Biophys. Chem.* **1991**, *20*, 267–298. (d) King, G.; Lee, F. S.; Warshel, A. *J. Chem. Phys.* **1991**, *95*, 4366–4377.

(8) Luzhkov, V.; Warshel, A. *J. Comput. Chem.* **1991**, *13*, 199–213.

(9) (a) Lee, F. S.; Chu, Z.-T.; Warshel, A. *J. Comput. Chem.* **1993**, *14*, 161–185. (b) Warshel, A.; Sussman, F.; King, G. *Biochemistry* **1986**, *25*, 8368–8372. (c) Warshel, A.; Parson, W. W. *Annu. Rev. Phys. Chem.* **1991**, *42*, 279–309. (d) Langen, R.; Brayer, G. D.; Berghuis, A. M.; McLendon, G.; Sherman, F.; Warshel, A. *J. Mol. Biol.* **1992**, *224*, 589–600.

(10) (a) Beveridge, D. L.; DiCapua, M. M. *Annu. Rev. Biophys. Biophys. Chem.* **1989**, *18*, 431–492. (b) Smith, P. E.; Pettit, B. M. *J. Phys. Chem.* **1994**, *98*, 9700–9711.

(11) (a) Sharp, K.; Honig, B. *Annu. Rev. Biophys. Biophys. Chem.* **1990**, *19*, 301–332. (b) Sharp, K. *J. Comput. Chem.* **1991**, *12*, 454–468. (c) You, T. J.; Harvey, S. C. *J. Comput. Chem.* **1993**, *14*, 484–501.

of the midpoint between the B and H macrocycles. The hydrogens in this part of the structure then were held fixed while the additional rotatable hydrogens outside the 40-Å sphere were equilibrated by a similar sequence of iterations. (The entire structure was used only to find the limiting value of $\Delta V_{Q\mu}$.) Separate Monte Carlo equilibrations were carried out for protein structures in which the ionizable amino acid side chains were in their neutral or charged forms; P, B, and H were in their neutral forms in all cases, and no electrolytes were included.

The equilibrated structure files were trimmed for electrostatic calculations on systems of various sizes. For calculations on the reaction $P^+B^-H \rightarrow P^+BH^-$, all atoms within a specified distance of the point midway between B and H were included (Figure 2B). For the reaction $P^*H \rightarrow P^+H^-$, we included all atoms within 32 Å of either the center of P or the center of H. Additional atoms were included as necessary to maintain electroneutrality of the simulation region when amino acid residues or pigments crossing the boundary were fragmented, or to include electrically charged functional groups such as $-CO_2^-$ in their entirety if any one of their atoms was within the region.

The calculations on ionized systems considered the side chains of all Asp, Glu, Arg, and Lys residues other than Glu(L)104 within the structural model, but did not ordinarily include net charges on N-terminal amino and C-terminal carboxyl groups. (The γ carboxylic acid group of Glu(L)104 is unlikely to ionize because it is hydrogen-bonded to the ring-V keto group of H.[1a]) The atomic charges of the electron carriers were as given previously.[3b] The positive charge of P^+ was distributed equally between the two BChls. A charge of +2.0 was used on the non-heme Fe when the amino acid side chains were ionized and +0.2 when they were neutral.

Because the mobile solvent molecules, most of the phospholipids or detergents, and the electrolytes in the solvent are not resolved in the X-ray structure, they must be added to the model. To represent these components, the trimmed protein was embedded in a cubic lattice with a spacing of 2.0 Å in regions within 14 Å of the center of the system and 3.0 Å elsewhere. The lattice was truncated to a sphere with a radius (R_{grid}) 10 Å greater than the radius of the trimmed protein (see Figure 2). (Further increases in R_{grid} had no significant effect on the results.) Grid points within the van der Waals exclusion radius of a crystallographic atom were deleted. The effect of the solvent and lipids in the volume elements associated with the remaining points was treated by a variation of the original PDLD approach (see the Appendix). This was done by assigning an atomic polarizability (κ_i, Å^3) to each volume element and obtaining the induced dipole (μ_i) at the grid point by an iterative solution of the expression

$$\mu_i = \kappa_i \xi_i \tag{5a}$$

$$= K v_i \xi_i \tag{5b}$$

Here v_i is the volume of the element represented by grid point i (8 Å^3 in the fine grid and 27 Å^3 in the coarse grid), ξ_i is the electrical field (e·Å^{-2}) at point i from the charges and induced dipoles of the protein atoms, electrolytes, and other grid points (excluding the nearest neighboring points), and K is a dimensionless coefficient that depends on the model of the solvent. V_{H_2O} for a particular charge-transfer state is given by

$$V_{H_2O} = \frac{C}{2}\sum_i \mu_i \xi_i = \frac{C}{2}\sum_i \kappa_i |\xi_i|^2 \tag{6}$$

where the sums run over all the grid points representing volume elements that are assumed to be occupied by mobile water molecules. V_{memb} is obtained similarly by summing over points representing regions occupied by lipids (see below).

To model water, the value of K in eq 5b was set at 0.256. This value was optimized, as described in the Appendix, by calculating the solvation energies of monovalent ions and the dielectric constant for interactions of ions in solution.

Both neutron diffraction measurements[12a] and theoretical considerations based on solvation free energies of the amino acid side chains[12b] suggest that the hydrophobic core of the reaction center is surrounded mainly by a belt of phospholipid side chains or detergents, rather than by bulk water. To examine the dielectric effects of these lipids, we used two different models. In the first model, all of the grid points between two parallel planes located approximately at the edges of the reaction center's transmembrane α-helices (region 2 in Figure 2B) were assigned a relatively low polarizability coefficient (K) of either 0.05968 or 0.1194. These coefficients correspond, respectively, to a macroscopic dielectric constant of 2 or 4 in the Clausius–Mosotti equation:[3b,7a]

$$\kappa_i = \{3(\epsilon - 1)/4\pi(\epsilon + 2)\} v_i \tag{7}$$

Grid points on either side of the nonpolar region 2 (region 3 in Figure 2B) were assigned the higher polarizability used to model water (K = 0.256) and also were considered to be accessible to electrolytes in the solvent (see below). Because the exact width of the hydrophobic belt of lipids surrounding the reaction center is uncertain, we carried out separate calculations on models in which the central region had widths of either 25 or 40 Å (see Figure 2A). The neutron diffraction measurements[12a] suggest that the width is about 25 Å, while arguments based on the solvation free energies[12b] favor a belt of about 40 Å.

In the model just described, cavities and crevices in the nonpolar region of the protein (region 1 in Figure 2B) are occupied by solvent with the same low polarizability as the external material in region 2, whereas cavities in the more polar domains on either side (Figure 2B, region 1′) are filled with water. This treatment could underestimate the dielectric effects of any mobile water molecules that actually reside in region 1. We therefore used a second procedure to identify internal cavities in region 1 and to examine the effects of changing the polarizability assigned to their contents. A grid first was constructed to represent the solvent surrounding the protein, and a 25-Å hydrophobic belt was formed as described above. Grid points at the periphery of region 2 (within the hydrophobic belt but well outside the trimmed protein) were assigned to represent nonpolar lipid side chains and were modeled with K = 0.1194. This set of points then was enlarged to include all other grid points in region 2 that were among the nearest neighbors of any member of the initial set. This procedure was continued iteratively until additional iterations no longer increased the set. Points that could not be connected to the lipid side chains in this way were taken to represent internal cavities of the protein. Separate calculations were done in which these volume elements were assigned a polarizability coefficient of 0, 0.1194, or 0.256. With a protein model that had been trimmed to a radius of 32 Å, this procedure typically identified about 50 scattered grid points in cavities that were isolated by the protein from the bulk lipid region; most of the cavities were large enough to hold only one or two molecules of water. The number of grid points identified varied by about ±5 if the origin of the grid was shifted randomly with respect to the center of the system.

The effects of induced dipoles in the protein (ΔV_{ind}) were evaluated by using an atomic polarizability of 1.3 Å^3 for all non-hydrogen atoms in the crystal structure, and zero for hydrogens. Because the density of non-hydrogen atoms inside the protein is approximately 0.0538 atom·Å^{-3}, this treatment is comparable to using eq 5 with K = 0.0699 (1.3 × 0.0538), which corresponds to $\epsilon \approx 2.2$ in the Clausius–Mosotti equation.

In most of the calculations, the O and H atoms of the water molecules seen in the crystal structure[1a] were treated in the same manner as the other crystallographic atoms, after the Monte Carlo procedure had been used to optimize the orientations of the hydrogens with respect to the charges of the protein and the chromophores in the state PBH. The relatively low atomic polarizabilities of 1.3 Å^3 assigned to the O atoms in the calculation of ΔV_{ind} could underestimate dielectric effects of water molecules that have some rotational mobility. We therefore also carried out calculations in which the atomic charges of the crystallographic water molecules were set to zero and the O atoms were given a polarizability of 2.16 Å^3 consistent with mobile water. This second treatment would overestimate the dielectric effects of water molecules whose rotational motions are restricted by, for example, hydrogen bonding to the protein. The results of the two treatments thus probably bracket the correct effects of the bound water molecules.

To ensure self-consistent interactions between the induced dipoles of the protein and solvent, the calculations of ΔV_{ind}, ΔV_{H_2O}, and ΔV_{memb} were combined in a single loop of the program. (In previous versions

(12) (a) Roth, M.; Lewit-Bentley, A.; Michel, H.; Deisenhofer, J.; Huber, R. *Nature* **1989**, *340*, 659–662. (b) Yeates, T. O.; Komiya, H.; Rees, D.; Allen, J. P.; Feher, G. *Proc. Natl. Acad. Sci. U.S.A.* **1987**, *84*, 6438–6442.

of the PDLD program, these terms were evaluated independently and then given first-order corrections for their interactions with each other.) The local-reaction-field (LRF) method[13] was not used in the calculations described in this section, and there was no cutoff distance for electrostatic interactions; rather, the interactions were reevaluated for all pairs of atoms and grid points in the system on each iteration of the loop.

Mobile electrolytes were treated by assigning a self-consistent set of net charges to the grid points that represented mobile water or polar regions of the membrane. The net charge at point i was

$$\phi_i = \frac{N_c v_i}{\sum_k v_k} \frac{\exp(-\psi_i/k_B T)}{\exp(-\psi_k/k_B T)} - \frac{N_a v_i}{\sum_k v_k} \frac{\exp(\psi_i/k_B T)}{\exp(\psi_k/k_B T)} \quad (8)$$

Here N_c and N_a are the total numbers of (monovalent) electrolyte cations and anions, respectively, in the model and ψ_i is the potential at point i due to the charges of the protein atoms, the electron carriers, and the other grid points.[9a,14] The electric potentials in eq 8 were evaluated by using a macroscopic dielectric constant of 60. This was high enough to keep all the $|\phi_i| \ll 1.0$, which is necessary for a stable solution. The ratios of N_c and N_a to the total volume accessible to the electrolytes were set for an ionic strength of 0.1 M when the net charge on the protein was zero, with additional counterions as needed to maintain electrical neutrality of the entire system when the protein was charged. This treatment of N_c and N_a somewhat overestimates the total number of counterions that would actually be found in a finite region around a charged protein; however, the error will be small if the ionic strength is sufficiently high and the electrolyte-accessible volume sufficiently large. The net charges at the grid points were obtained by solving eq 8 iteratively, and then were held constant during the iterative calculations of induced dipoles in the protein, solvent, and membrane. However, the fields from the electrolytes were included explicitly (using a dielectric constant of 1) in the calculations of all induced dipoles. This procedure can be viewed as using a macroscopic approach for evaluating ϕ_i while retaining a microscopic approach for examining the effect of ϕ_i on the rest of the system. Because little translational diffusion of the electrolytes would occur on the time scale of the electon-transfer reactions, the same set of charges was used for both P^+B^-H and P^+BH^-. Except where indicated in connection with models of a frozen solvent (see below), the charges were calculated for the system in the state P^+B^-H. For comparison, we also carried out calculations on models that had no electrolyte charges.

ΔV_{bulk} was evaluated with the expression

$$\Delta V_{bulk} = -C\left\{\left(\frac{Q(3)^2 - Q(2)^2}{2b}\right)\left(\frac{\epsilon_{bulk} - 1}{\epsilon_{bulk}}\right) + \left(\frac{|\mu(3)|^2 - |\mu(2)|^2}{b^2}\right)\left(\frac{\epsilon_{bulk} - 1}{2\epsilon_{bulk} + 1}\right)\right\} \quad (9)$$

Here b is the radius of the simulation sphere within which the protein, solvent, and electrolytes are treated microscopically, $Q(3)$ and $Q(2)$ are the total charges of the microscopic system in the states P^+BH^- and P^+B^-H, including the protein and electrolytes as well as the electron carriers, $\mu(3)$ and $\mu(2)$ are the electric dipoles of the system in these states, and ϵ_{bulk} is the dielectric constant of the bulk solvent surrounding the system. We used $\epsilon_{bulk} = 80$. The radius b is $R_{grid} + s_{grid}/2$, where s_{grid} is the spacing of the coarse grid (3 Å). The dipoles $\mu(3)$ and $\mu(2)$ are given by sums of the form

$$\mu = \sum_i (q_i \mathbf{r}_i + \mu_i) \quad (10)$$

where q_i is the charge at protein atom or grid point i, $\mathbf{r}_i$ is a vector from the center of the grid to the atom or grid point, and μ_i is the induced dipole at the atom or point.

In general, ΔV_{bulk} for a charge-shift reaction such as $P^+B^-H \rightarrow P^+BH^-$ depends on the net charge within the simulation sphere, even if the total charge does not change in the reaction.[7a] This may be clearer if the dipole μ defined by eq 10 is written as

$$\mu = Q\mathbf{r}_Q + \mu_o \quad (11)$$

where Q is the net charge of the system, $\mathbf{r}_Q$ is the location of the center of charge relative to the center of the grid, and μ_o is the dipole given by eq 10 when the grid is centered at the center of charge (or with the grid centered arbitrarily if $Q = 0$). ΔV_{bulk} depends on the change in $|\mu|^2$, which can be very different from the change in $|\mu_o|^2$ depending on Q and $\mathbf{r}_Q$. In most of the present calculations, electrolyte counterions were included to keep $Q = 0$ even though trimming the protein to various sizes caused the net charge of the protein to vary from -5 to $+2$. The effects of changing the protein's charge were absorbed largely in ΔV_{ions}.

The values obtained for ΔV_{H_2O}, ΔV_{memb}, ΔV_{ions}, and ΔV_{bulk} depend to some extent on the positioning of the grid used to represent the membrane or solvent. Each value of ΔG_{sol}^{pro} or ΔG_{sol}^{ref} presented below is the mean of results obtained with at least 10 different grids centered at random points up to 2 Å from the center of the rest of the system. Where not given below, the standard errors of the means typically were about ±0.7 kcal/mol for the models with water as the solvent and ±0.4 kcal/mol for the models that included a membrane.

In all the models described above, the atomic polarizabilities (κ_i) used to represent induced dipoles in the solvent are based on low-frequency dielectric properties of liquid water (see the Appendix). The induced dipoles therefore pertain to systems in which the water has undergone complete dielectric relaxation, while the protein atoms remain in their crystallographic positions. In the actual system, part of the dielectric relaxation of the protein, membrane, and water may occur slowly, relative to the rate of electon transfer.[17] We explored this point by using the following two-step procedure to model systems in which the electrolytes and all the induced dipoles are frozen in their initial configurations. In the first step, the electrolyte charges and the induced dipoles of the water, membrane, and protein were calculated just as described above, but for the system in the state PBH that precedes the initial charge-separation reaction. All of the induced dipoles then were scaled in magnitude by the factor $K_{lf}/K = (K - K_{hf})/K$, where K is the total atomic polarizability coefficient parametrized as described above, K_{hf} is the "high-frequency" or "optical" polarizability coefficient of 0.0597 that corresponds to a dielectric constant of 2 in the Clausius–Mosotti equation, and K_{lf} is the "low-frequency" polarizability coefficient representing slower, orientational dielectric effects. The electrolyte charges and the low-frequency induced dipoles were held constant for the second step of the procedure. In the second step, new high-frequency induced dipoles were calculated for the protein, membrane, and solvent in the states P^+B^-H and P^+BH^-. This was done by using $K = K_{hf}$ but requiring each high-frequency dipole to respond to the total electric field from the electrolytes and low-frequency dipoles, in addition to the fields from the atomic charges of the protein and electron carriers and the other high-frequency dipoles. ΔV_{bulk} for the frozen system was calculated with the expression

(13) Lee, F. S.; Warshel, A. *J. Chem. Phys.* **1992**, *97*, 3100–3107.
(14) Klein, B. J.; Pack, G. R. *Biopolymers* **1983**, *22*, 2331–2352.
(15) (a) Warshel, A. *J. Phys. Chem.* **1982**, 86, 2218–2224. (b) Warshel, A.; Hwang, J.-K. *J. Chem. Phys.* **1986**, *84*, 4938–4957. (c) Hwang, J.-K.; Warshel, A. *J. Am. Chem. Soc.* **1987**, *109*, 715–720. (d) Hwang, J.-K.; King, G.; Creighton, S.; Warshel, A. *J. Am. Chem. Soc.* **1988**, *110*, 5297–5311. (e) King, G.; Warshel, A. *J. Chem. Phys.* **1990**, *93*, 8682–8692.
(16) (a) Beroza, P.; Fredkin, D. R.; Okamura, M. Y.; Feher, G. *Proc. Natl. Acad. Sci. U.S.A.* **1991**, *88*, 5804–5808. (b) Yang, A.-S.; Gunner, M. R.; Sampogna, R.; Sharp, K.; Honig, B. *Proteins: Struct., Funct., Genet.* **1993**, *15*, 252–265. (c) Gunner, M. R.; Honig, B. In *The Photosynthetic Bacterial Reaction Center. II. Structure, Spectroscopy and Dynamics;* Breton, J., Verméglio, A., Eds.; Plenum Press: New York, 1992; pp 403–410.
(17) (a) Vos, M. H.; Lambry, J.-C., Robles, S. J.; Youvan, D. C.; Breton, J.; Martin, J.-L. *Proc. Natl. Acad. Sci. USA* **1991**, *88*, 8885–8889. (b) Vos, M. H.; Jones, M. R.; Hunter, C. N.; Breton, J.; Lambry, J.-C.; Martin, J.-L. *Biochemistry* **1994**, *33*, 6750–6757. (c) Peloquin, J. M.; Williams, J. C.; Lin, X.; Alden, R. G.; Taguchi, A. K.; Allen, J. P.; Woodbury, N. W. *Biochemistry* **1994**, *33*, 8089–8100.
(18) (a) Komiya, H.; Yeates, T. O.; Rees, D. C.; Allen, J. P.; Feher, G. *Proc. Natl. Acad. Sci. U.S.A.* **1988**, *85*, 9012–9016.

$$\Delta V_{\text{bulk}}^{\text{frozen}} = -C\mu(0)\cdot\left(\frac{\mu(3)-\mu(2)}{b^2}\right)\left(\left(\frac{\epsilon_{\text{bulk}}-1}{2\epsilon_{\text{bulk}}+1}\right)-\left(\frac{\epsilon_\infty-1}{2\epsilon_\infty+1}\right)\right) - C\left(\frac{|\mu(3)|^2-|\mu(2)|^2}{b^2}\right)\left(\frac{\epsilon_\infty-1}{2\epsilon_\infty+1}\right) \quad (12)$$

Here $\mu(0)$ is the dipole of the system in the state PBH, including the contributions from the electrolyte charges and low-frequency induced dipoles. The second term on the right side of eq 12 represents the interactions of $\mu(3)$ and $\mu(2)$ with high-frequency induced dipoles in the bulk solvent. The first term on the right-hand side of eq 12 represents the interaction of $\mu(3)$ and $\mu(2)$ with the low-frequency induced dipoles that are frozen in the bulk solvent before the electron-transfer reactions.

The changes in solvation energy for reduction of bacteriochlorophyll *b* (BChl) or bacteriopheophytin *b* (BPh) in solution [$G_{\text{sol}}^{\text{ref}}(\text{B}^-) - G_{\text{sol}}^{\text{ref}}(\text{B})$ and $G_{\text{sol}}^{\text{ref}}(\text{H}^-) - G_{\text{sol}}^{\text{pro}}(\text{H})$ in Figure 1] were calculated in essentially the same manner as $\Delta G_{\text{sol}}^{\text{pro}}$, using the treatment described above for a relaxed polar solvent containing electrolytes. Acetonitrile was included as an axial ligand in the model of bacteriochlorophyll and was treated as part of the solvent.[3b] The electrolyte charges (ϕ_i) on the grid points were evaluated separately for the neutral molecule and the reduced species. These calculations were done in two different ways: (i) The total numbers of electrolyte anions and cations were held constant when the molecules were reduced. This procedure left the individual reactions BChl → BChl$^-$ and BPh → BPh$^-$ balanced with respect to mass but unbalanced with respect to charge. Charge balance was restored when the individual reactions were combined into $\Delta G_{\text{sol}}^{\text{ref}}$ for the overall reference reaction BPh$^-$ + BChl → BPh + BChl$^-$. In this approach, ΔV_{bulk} for each of the individual reactions includes a term that reflects the change in net charge Q from 0 to −1 [the first term on the right in eq 9 becomes $-C(1 - 1/\epsilon_{\text{bulk}})/2b$]. (ii) Additional counterions were provided to maintain electrical neutrality when the bacteriochlorophyll or bacteriopheophytin was reduced in the individual reactions. This second approach leaves the individual reactions unbalanced with regard to mass (BPh → BPh$^-$ + C$^+$ and BChl → BChl$^-$ + C$^+$, where C$^+$ is the counterion), but mass balance is restored when the calculations are combined into $\Delta G_{\text{sol}}^{\text{ref}}$. Both methods gave $\Delta G_{\text{sol}}^{\text{ref}} = -11.21 \pm 0.36$ kcal/mol. The convergence of the results obtained by the two methods illustrates the overall robustness of the calculations and the complementarity of the multiple terms that contribute to the solvation energy (eq 3).

FEP/MD Simulations. The MD simulations used the ENZYMIX force field with surface-constrained all-atom solvent (SCAAS) boundary conditions.[9a] The system studied was represented by an inner spherical region where the molecular structure of the reaction center was treated explicitly, surrounded by a boundary region that constrained the inner atoms to behave as though they were part of an infinite system.[9a,b] The SCAAS boundary conditions are important because the periodic boundary conditions that frequently are used in molecular-dynamics simulations do not properly represent the polarization of the solvent around a charged molecule.[9a,b] A 45-Å belt of lipids surrounding the protein was modeled by a grid of uncharged atoms with an atomic polarizability of 1.3 Å^3 ($0.0303v_i$) and a van der Waals interaction potential that kept the lipid atoms 3.5 Å from each other and from the closest protein atom. Water molecules were inserted into any remaining cavities of the protein, but no electrolyte ions were included. Induced dipoles in the protein were evaluated as described,[9a] except that a distance-dependent attenuation of the fields from nearby atoms was replaced by an explicit exclusion of the fields from 1−2, 1−3, and 1−4 bonded atoms. The treatment of BChl−histidine interactions was modified to maintain a distance of 2.0 Å between the Mg and histidine $N_{\epsilon 2}$. For most of the calculations, the protein−membrane system was trimmed to a sphere with a radius of 25 Å, and the inner region in which the protein and water atoms were unconstrained and an all-atom model was used for mobile water molecules had a radius of 20 Å. The region outside the larger sphere was treated as a continuum with the dielectric constant of bulk water.

Free energy surfaces were calculated by the free-energy-perturbation (FEP)/umbrella sampling method.[3a,9c,15] In this approach, the reaction coordinate (x) for a transition between two charge-transfer states (i and j) is taken to be the change in potential energy [$E_j(t) - E_i(t)$] associated with moving an electron from the donor to the acceptor. This energy gap fluctuates with time as the atomic coordinates change during a molecular-dynamics simulation. A free energy function of the reaction coordinate is defined as $\Delta g(x_u) = -k_B T \ln[\mathscr{P}(x_u)]$, where $\mathscr{P}(x_u)$ is the probability that the energy gap is within a small region ($\pm\Delta x/2$) around a particular value (x_u). This function can be evaluated by propagating molecular-dynamics trajectories on a series of mapping potential energy surfaces

$$E_v = (1 - \theta_v)E_i + \theta_v E_j \quad (13)$$

with the mapping parameter θ_v increasing stepwise from 0 to 1. The free energy function for the system in state i is given by[15]

$$\Delta g_i(x_u) \approx -k_B T \ln[\langle \delta(x - x_u) \exp\{-[E_i(t) - E_w(t)]/k_B T\}\rangle_w \mathscr{P}_w] \quad (14)$$

Here E_w is a mapping potential that forces the atomic coordinates and induced electric dipoles to evolve so that the energy gap frequently intersects x_u, $\langle\ \rangle_w$ denotes a time average over a trajectory on E_w, the delta function $\delta(x - x_u)$ is assigned a value of 1 if $|x(t) - x_u| \le \Delta x/2$ and zero otherwise, and

$$\mathscr{P}_w = \prod_{v=0}^{w-1} \langle \exp\{-[E_{v+1}(t) - E_v(t)]/k_B T\}\rangle_v \quad (15)$$

In the present studies, we changed θ_v from 0 to 1 in six steps with MD simulations of 10 ps each, following an initial equilibration for 10 ps. The MD trajectories were propagated at 300 K with 1-fs time steps. The width of the delta function (Δx) was chosen to divide the total range of x covered during all the trajectories into 20 equal intervals. The FEP/MD calculations made use of the local-reaction-field (LRF) method, which provides a rapid yet reliable way to treat long-range electrostatic interactions.[13] The reorganization energy for conversion of the system from state i to state j is $\lambda_{ij} = \Delta g_j(x_o^i) - \Delta g_j(x_o^i)$, where $\Delta g_i(x_o^i)$ is the minimum value of $\Delta g_i(x)$ (*i.e.*, where x_o^i is the most probable value of x during a trajectory on E_i).

Results

Establishing the Stability of the Calculations. As pointed out above, it is important to demonstrate that the results of an electrostatics calculation are independent of the size of the region that is included explicitly in the model. The best way to explore the requirements for stable and reliable electrostatic calculations is to consider specific test cases. We have done this by calculating the change in electrostatic free energy for the reaction P$^+$B$^-$H → P$^+$BH$^-$ ($\Delta G_{\text{sol}}^{\text{pro}}$), using models in which the protein was trimmed to spheres of various sizes. The models also incorporated a variety of treatments of the ionizable amino acid residues, and of the solvent or membrane surrounding the protein, to determine the upper and lower limits of the effects of these components.

Consider first PDLD-type calculations on models in which all of the ionizable amino acid residues are in their neutral states, leaving the effects of ionizing these residues to be examined later. This was the approach used in the previous studies by Creighton et al.[3a] and Parson et al.[3b] The open circles in Figure 3A show the values of $\Delta V_{Q\mu}$ (the contributions to $\Delta G_{\text{sol}}^{\text{pro}}$ from direct electrostatic interactions of B and H with the protein, P$^+$, and crystallographic water atoms in the absence of dielectric screening by the rest of the system) as a function of the amount of the protein included in the model. The filled symbols show the complete $\Delta G_{\text{sol}}^{\text{pro}}$, including the dielectric effects of the protein, solvent, and electrolytes. The filled squares were obtained with models in which the protein was surrounded by water, the filled circles with models that included a membrane with a nonpolar region of 25 Å. With both of these models, the calculated values of $\Delta G_{\text{sol}}^{\text{pro}}$ become progressively less

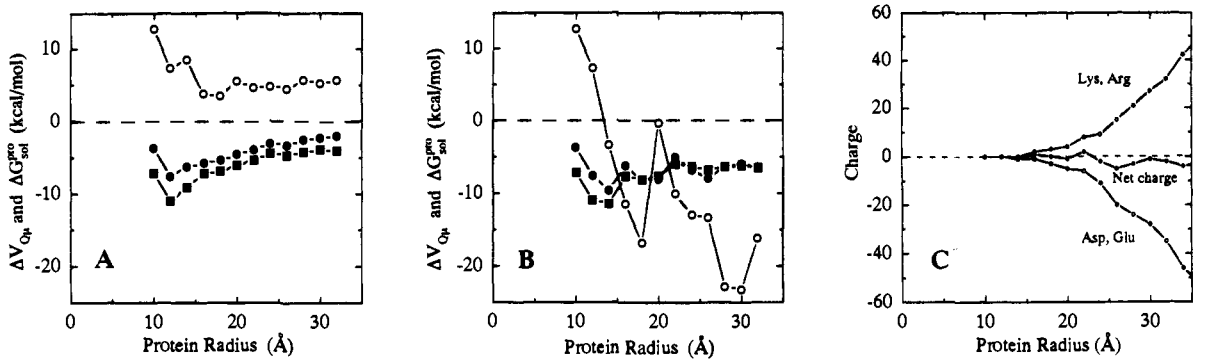

Figure 3. (A) Calculated values of $\Delta V_{Q\mu}$ (○) and ΔG_{sol}^{pro} (■, ●) for $P^+B^-H \rightarrow P^+BH^-$ in models with all ionizable amino acid residues in their neutral forms: ■, protein in water; ●, protein in a membrane with a 25-Å hydrophobic region and an atomic polarizability (κ_i) of $0.1194v_i$. The abscissa is the radius of the region in which the protein and water atoms of the crystal structure were treated explicitly. For all of the calculations, the non-heme Fe atom was given an effective charge of +0.2 and the positive charge of P^+ was divided equally between the two bacteriochlorophylls. (B) Same as (A) except that all Lys, Arg, and Asp residues, and all Glu residues except Glu (L)104 were ionized. (C) Total charges of ionizable residues in the models used for the calculations shown in (B).

Table 1. Contributions to ΔG_{sol}^{pro} and ΔG° for $P^+B^-H \rightarrow P^+BH^-$ (ΔG_{23}°) in Various PDLD-Type Models of the Protein and Solvent[a]

model[b]									
charge	w	K	$\Delta V_{Q\mu}$	ΔV_{ind}	$\Delta V_{H_2O/memb}$[c]	ΔV_{ions}	ΔV_{bulk}	ΔG_{sol}^{pro}	ΔG_{23}°
I	0		−16.2	−3.8	8.6	5.0	−0.2	−6.5 ± 0.6	−4.9 ± 0.7
I	25	0.119	−16.2	−3.1	7.2	4.3	1.4	−6.4 ± 0.3	−4.8 ± 0.5
I	25	0.060	−16.2	−2.9	6.4	4.3	2.4	−6.0 ± 0.3	−4.4 ± 0.5
I	40	0.119	−16.2	−2.7	6.5	3.1	1.6	−7.7 ± 0.3	−6.1 ± 0.5
I	40	0.060	−16.2	−2.2	4.8	3.1	2.6	−8.0 ± 0.2	−6.4 ± 0.4
N	0		5.6	−6.2	−2.9	−0.4	−0.2	−4.1 ± 0.6	−2.5 ± 0.7
N	25	0.119	5.6	−7.1	−1.3	0.4	0.3	−2.1 ± 0.3	−0.5 ± 0.5
N	25	0.060	5.6	−7.9	−1.0	0.7	0.6	−2.0 ± 0.3	−0.4 ± 0.5
N	40	0.119	5.6	−7.3	−1.1	0.7	0.4	−1.7 ± 0.3	−0.1 ± 0.5
N	40	0.060	5.6	−8.0	−0.4	0.7	0.7	−1.4 ± 0.2	0.2 ± 0.4

[a] Energies are given in kilocalories per mole and are averages of results for 10 different grids. The uncertainties in ΔG_{sol}^{pro} and ΔG_{23}° are standard errors of the means. The values of ΔG_{23}° include ΔE^{gas} (3.4 ± 0.4 kcal/mol) and ΔV_{QQ} (−1.8 kcal/mol). [b] The protein was trimmed to a radius of 32 Å about a point midway between B and H. The side chains of the Lys, Arg, Asp, and Glu residues other than Glu(L)104 were either ionized (I) or neutral (N), as indicated in the charge column. The nonpolar region of the membrane (Figure 2, region 2) had a width (w) of 0, 25, or 40 Å, and the atomic polarizability coefficients (K) for volume elements in this region were as indicated. $K = 0.060$ corresponds to a bulk dielectric constant (ϵ) of 2, $K = 0.119$, to $\epsilon = 4$. Volume elements in region 3 (see Figure 2) were assigned atomic polarizabilities of $0.256v_i$. Volume elements in cavities in regions 1 and 1′ of the protein were treated in the same manner as volume elements in regions 2 and 3, respectively. In the models with $w = 0$ the protein was embedded in water ($K = 0.256v_i$). [c] $\Delta V_{H_2O/memb}$ is the sum of ΔV_{H_2O} and ΔV_{memb}.

negative as the radius of the trimmed protein is increased from 12 to 20 Å. Further increases in size have relatively little effect.

Parallel calculations were performed on systems in which all of the Lys, Arg, and Asp residues, and all the Glu residues except Glu(L)104, were in their charged states (Figure 3B,C). Ionizing these residues changes $\Delta V_{Q\mu}$ considerably and makes it extremely sensitive to the amount of protein included in the model. In some cases $\Delta V_{Q\mu}$ differs by more than 25 kcal/mol from the value obtained when the ionizable groups are taken to be neutral. (Compare the open circles in Figure 3B with those in Figure 3A, particularly for the models with protein radii of 28−30 Å). The systems with a radius of 10 or 12 Å necessarily give identical results in the two treatments because these small regions of the reaction center have no ionizable amino acids.) The sensitivity of $\Delta V_{Q\mu}$ to the size of the model and to the charges of the ionizable groups is expected because unscreened electrostatic interactions fall off slowly with distance.

When the dielectric effects of the protein, solvent, and electrolytes are taken into account by representing the contributions explicitly, the calculated values of ΔG_{sol}^{pro} become remarkably insensitive to the size of the model. With water as the solvent (Figure 3B, filled squares), ΔG_{sol}^{pro} again converges when the radius of the trimmed protein is about 20 Å and the asymptotic value differs by only about 3 kcal/mol from the value obtained with the ionizable amino acids in their neutral states. The results for models that include a nonpolar belt (Figure 3B, filled circles) fluctuate slightly more than those for the water model, but converge on essentially the same value of ΔG_{sol}^{pro}.

Table 1 lists the contributions to ΔG_{sol}^{pro} for a variety of models in which the protein is embedded either in water or in a membrane with a central, nonpolar region. Although $\Delta V_{Q\mu}$ varies from −16.2 to +5.6 kcal/mol depending on the charges assigned to the ionizable residues, the compensating effects of electrolyte counterions and induced dipoles in the solvent and protein keep the total ΔG_{sol}^{pro} relatively constant. Increasing the width of the membrane's nonpolar region from 25 to 40 Å has little effect when the ionizable groups of the protein are in their neutral states, but makes ΔG_{sol}^{pro} more negative by about 1.3 kcal/mol when these groups are ionized. Varying the atomic polarizability coefficient (K) of the volume elements in the nonpolar region from 0.060 to 0.119, corresponding to macroscopic dielectric constants of 2 and 4, does not change the results significantly.

Table 2 shows the effects of varying the treatment of internal cavities in the nonpolar region of the protein. The calculated values of ΔG_{sol}^{pro} vary over a range of only about 1 kcal/mol, depending on whether these cavities are left empty ($K^{cav} = 0$) or are filled with nonpolar material ($K^{cav} = 0.119$) or water ($K^{cav} = 0.256$). Replacing the crystallographic water molecules by induced dipoles with the same atomic polarizability as used for bulk water ($K = 0.256$) also has very little effect on the results.

Table 2. Contributions to ΔG_{sol}^{pro} and ΔG° for $P^+B^-H \rightarrow P^+BH^-$ (ΔG_{23}°) with Various Treatments of Internal Cavities in Nonpolar Regions of the Protein[a]

model[b]								
charge	K^{cav}	$\Delta V_{Q\mu}$	ΔV_{ind}	$\Delta V_{H_2O/memb}$[c]	ΔV_{ions}	ΔV_{bulk}	ΔG_{sol}^{pro}	ΔG_{23}°
I	0	−16.2	−2.9	6.7	4.6	2.4	−5.8 ± 0.4	−4.2 ± 0.6
I	0.119	−16.2	−3.1	7.2	4.3	1.4	−6.4 ± 0.3	−4.8 ± 0.5
I	0.256	−16.2	−3.2	6.7	4.5	1.4	−6.7 ± 0.6	−5.1 ± 0.7
I	0.256[d]	−14.4	−4.3	5.5	4.8	1.6	−6.7 ± 0.6	−5.1 ± 0.7
N	0	5.6	−8.0	−0.3	0.7	0.6	−1.2 ± 0.2	0.4 ± 0.4
N	0.119	5.6	−7.1	−1.3	0.4	0.3	−2.1 ± 0.3	−0.5 ± 0.5
N	0.256	5.6	−6.8	−2.3	0.4	0.3	−2.8 ± 0.6	−1.2 ± 0.7
N	0.256[d]	5.9	−7.2	−3.3	0.7	0.4	−3.6 ± 0.6	−2.0 ± 0.7

[a] Energies are given in kilocalories per mole and are averages of results for 10 different grids. The uncertainties in ΔG_{sol}^{pro} and ΔG_{23}° are standard errors of the means. The values of ΔG_{23}° include ΔE^{gas} (3.4 ± 0.4 kcal/mol) and ΔV_{QQ} (−1.8 kcal/mol). [b] The protein was trimmed to a radius of 32 Å about a point midway between B and H. The ionizable side chains were either ionized (I) or neutral (N), as indicated. All models described in this table included a membrane with a 25-Å nonpolar region; κ_i was $0.1194v_i$ in region 2 and 0.256 in region 3. The volume elements associated with internal cavities in the nonpolar region of the protein (Figure 2B, region 1) were assigned atomic polarizability coefficients (K^{cav}) of 0, 0.119, or 0.256 as indicated; those in region 1′ were given coefficients of 0.256. [c] $\Delta V_{H_2O} + \Delta V_{memb}$. [d] All X-ray waters also treated as induced dipoles. Fixed charges of the water atoms were omitted, and O atoms were assigned an atomic polarizability of 2.16 Å^3.

Table 3. ΔG_{sol}^{pro} for $P^+B^-H \rightarrow P^+BH^-$ in Other Variations in the PDLD-Type Model[a]

model[b]	$\Delta V_{Q\mu}$	ΔV_{ind}	$\Delta V_{H_2O/memb}$[c]	ΔV_{ions}	ΔV_{bulk}	ΔG_{sol}^{pro}
			Ionized			
standard model[d]	−16.16	−3.12	7.21	4.26	1.40	−6.40 ± 0.32
(L)168 $N_{\epsilon 2}$ H[e]	−15.47	−3.13	5.55	5.18	1.33	−6.54 ± 0.62
no electrolytes	−16.16	−2.76	9.08	0.00	0.94	−8.89 ± 0.50
frozen[f]	−16.16	−1.85	1.42	3.82	0.73	−12.05 ± 0.60
			Neutral			
standard model[d]	5.63	−7.05	−1.31	0.39	0.28	−2.07 ± 0.25
(L)168 $N_{\epsilon 2}$ H[e]	6.54	−7.86	−2.45	0.87	0.39	−2.51 ± 0.42
no electrolytes	5.63	−6.90	−2.03	0.00	0.21	−3.09 ± 0.55
frozen[f]	5.63	−3.88	−1.66	0.09	0.01	0.19 ± 0.74

[a] Energies are given in kilocalories per mole and are averages of results for 10 different grids. The uncertainties in ΔG_{sol}^{pro} are standard errors of the means. [b] The protein was trimmed to a radius of 32 Å about a point midway between B and H. The ionization states of the ionizable side chains were as indicated. All models included a membrane with a 25-Å nonpolar region with $K = 0.119$. [c] $\Delta V_{H_2O} + \Delta V_{memb}$. [d] Same as the models with $w = 25$, $K = 0.119$, and $K^{cav} = 0.119$ in Tables 1 and 2 (includes electrolytes and has Nδ of histidine (L)168 protonated). [e] $N_{\epsilon 2}$ of histidine (L)168 protonated. [f] Low-frequency dipoles of protein, membrane, and water frozen (see text).

Table 3 shows the effects of several other variations in the model. Omitting electrolytes makes the calculated values of ΔG_{sol}^{pro} somewhat more negative and more sensitive to the charges of the ionizable residues. Changes in other terms compensate for about half of the loss of ΔV_{ions} in the model with ionized side chains, but overcompensate for this loss in the model with neutral side chains. The magnitude of ΔV_{ions} is, as expected, considerably larger when the ionizable side chains are charged. The models identified in Table 3 as "(L)-168 $N_{\epsilon 2}$ H" show the effects of tautomerization of the side chain of histine (L)168. In the models used in most of our calculations the $N_{\epsilon 1}$ of all histidine side chains was protonated and $N_{\epsilon 2}$ was unprotonated. The actual protonation state probably is reversed in histidine (L)168 because a proton on $N_{\epsilon 2}$ forms a hydrogen bond to the acetyl group of one of the BChls of P. However, models with the two tautomers gave similar values of ΔG_{sol}^{pro} for the process of interest here. The effects of tautomerizing or charging other individual histidine residues will be considered in more detail elsewhere. The calculations on "frozen" systems (Table 3) will be discussed below.

In order to use eqs 1 and 2 to evaluate the change in free energy for the reaction $P^+B^-H \rightarrow P^+BH^-$ (ΔG_{23}°), we also require ΔG_{sol}^{ref} for the reference reaction $BChl^- + BPh \rightarrow BChl + BPh^-$. ΔG_{sol}^{ref} was obtained by PDLD-type calculations on BPh *b* and BChl *b* in a polar solvent containing electrolytes, with acetonitrile as the axial ligand of BChl *b*. Two alternative treatments of the counterions (see the Methods) both gave −11.21 ± 0.36 kcal/mol. Combining this value with the experimentally measured term in eq 1, $\mathcal{F}[E_m^H - E_m^B] = 7.8$ kcal/mol,[3b,19] gives $\Delta E^{gas} = +3.4 \pm 0.4$ kcal/mol. Calculations on BPh *b* and BChl *b* in a polar solvent without electrolytes gave very similar results ($\Delta G_{sol}^{ref} = -12.1$ and $\Delta E^{gas} = +4.3$ kcal/mol.) ΔV_{QQ}, the change in direct electrostatic interactions between B and H, has been evaluated previously as −1.80 kcal/mol,[3b] and is constant in all the models considered here. The last columns in Tables 1 and 2 give the final values of ΔG_{23}° for the models that we explored most thoroughly. In the models with ionized side chains, ΔG_{23}° is calculated to be in the range of −5 kcal/mol, whereas the models with neutral side chains give values on the order of −1 kcal/mol.

Similar results were obtained in FEP/MD simulations (Table 4). These calculations gave values of about −9 kcal/mol for ΔG_{sol}^{pro} when the ionizable residues were charged, and about −3 kcal/mol when these residues were neutral. Variations in the treatment of the solvent in the protein's cavities, or decreasing the radius of the protein model from 25 to 20 Å, changed the results by ±2 kcal/mol (not shown). Models that included only the water molecules seen in the X-ray structure gave more negative values of ΔG_{sol}^{pro} that depended much more strongly on the charges assigned to the ionizable groups and the size of the model (see Table 4).

For the reference reaction $BChl^- + BPh \rightarrow BChl + BPh^-$, FEP/molecular-dynamics simulations with explicit SCAAS water molecules as the solvent, imidazole as the axial ligand of BChl *b*, and no electrolytes gave $\Delta G_{sol}^{ref} = -16.7 \pm 2$ kcal/mol.

(19) (a) Fajer, J.; Borg, D. C.; Forman, A.; Dolphin, D.; Felton, R. H. *J. Am. Chem. Soc.* **1973**, *95*, 2739–2740. (b) Fajer, J.; Davis, M. S.; Brune, D. C.; Spaulding, L. D.; Borg, D. C.; Forman, A. *Brookhaven Symp. Biol.* **1976**, *28*, 74–103.

Table 4. Model Dependence of ΔG_{sol}^{pro} and ΔG° for $P^+B^-H \rightarrow P^+BH^-$ (ΔG_{23}°) in FEP/MD simulations[a]

model[b]	charge[c]	ΔG_{sol}^{pro}	ΔG_{23}°
membrane and mobile water[d]	N	−3.3	3.8
	I	−9.1	−2.0
X−ray water only[e]	N	−12.4	−5.3
	I	−25.5	−18.4

[a] All energies are in kilocalories per mole and have estimated uncertainties of ±3 kcal/mol. The values of ΔG_{23}° include ΔE^{gas} (8.9 ± 2 kcal/mol) and ΔV_{QQ} (−1.8 kcal/mol). [b] The radius within which the protein−membrane system was treated explicitly (R_{4b} in Figure 3 of ref 9a) was 25 Å. This includes both the inner region of unconstrained protein atoms, which had a radius of 20 Å, and a shell of harmonically constrained atoms. [c] The ionizable side chains were either ionized (I) or neutral (N). [d] The membrane surrounding the nonpolar region of the protein was represented by a grid of weakly polarizable atoms (see text); mobile water molecules filled any available cavities in the more polar region. Mobile water molecules in the outer 5-Å shell of the system were modeled by Langevin dipoles; explicit, all-atom water models were used in the inner region of unconstrained atoms. [e] No mobile solvent or membrane.

When combined with $\mathcal{F}[E_m^H - E_m^B]$ (7.8 kcal/mol), this value leads to $\Delta E^{gas} = +8.9 \pm 2$ kcal/mol. The difference of about 5 kcal/mol between the values of ΔE^{gas} obtained in the FEP/MD calculations and in the PDLD-type calculations probably is due in part to the different methods of handling induced dipoles and to different constraints on the distance between B and its axial ligand (see the Methods). Because the same methods were used for the reference reaction as for the protein in each case, these differences largely cancel out in the final values of ΔG_{23}°. Adding the FEP/MD ΔE^{gas} and ΔV_{QQ} to the values of ΔG_{sol}^{pro} obtained in the FEP/MD simulations with the ionizable side chains charged and with the solvent and membrane treated explicitly gives $\Delta G_{23}^{\circ} \approx -2$ kcal/mol, with an uncertainty on the order of ±3 kcal/mol (see Table 4). With the ionizable side chains neutral, the calculated ΔG_{23}° is +4 ± 3 kcal/mol.

We conclude that electrostatic calculations on either static or dynamic models of the protein can give stable results with systems of relatively small size, provided that the dielectric effects of the surrounding medium are taken into account. Of course, establishing the stability of a calculation does not guarantee that the model used is physically realistic. Even after the results have converged, calculations that do not consider the effects of the solvent will overestimate the importance of long-range electrostatic interactions. Treatments that do include solvent, and thus converge smoothly, may or may not be quantitatively reliable depending on the dielectric properties assigned to the solvent and on the charges assigned to the ionizable amino acids. However, it is encouraging that including the solvent makes the final values of ΔG_{sol}^{ref} insensitive to variations in the details of the model.

Microscopic Treatments of Individual Ionized Groups. The results collected in Tables 1−4 show that taking all of the potentially ionizable Asp, Glu, Arg, and Lys residues to be in the charged forms leads to calculated solvation energies for $P^+B^-H \rightarrow P^+BH^-$ that are more negative than the values obtained when these residues are taken to be neutral. Although most of these residues are likely to be ionized at physiological pH, some of them probably are not.[3b,16] Assignments of the individual ionization states are difficult because the electric field at the site of a given residue depends on the ionization states of all the other residues as well as on the self-energy of each ionized residue.[7a,16] Determining the self-energies requires a separate calculation for each residue, and determining the interactions between the residues requires a calculation for each pair. However, one still can use a microscopic approach to estimate the effects that any particular group will have if it is ionized. We have done this for all the Lys, Arg, Asp, and Glu residues with ionizable functional groups within 20 Å of the point midway between B and H. The locations of these residues are shown in Figure 4. Arg(H)33 and Asp(H)36, which probably form an ion pair, were considered both individually and together, and Glu(M)232, which is a ligand of the non-heme Fe atom, was considered both individually and as a unit with the Fe. Table 5 gives the results of calculations on static models of the protein; Table 6 presents FEP/MD calculations on two representative residues, Asp(L)60 and Arg(L)103. The tables also give $\Delta\Delta V_{Q\mu}$, the effect of the ionizable group on the interaction energy in the absence of dielectric effects.

In the PDLD-type calculations (Table 5), the charges of the three ionizable residues closest to the center of the system, Asp(L)155, Arg(L)103, and Arg(L)135, are calculated to have potentially significant effects on ΔG_{sol}^{pro} even when the protein in the model is embedded in water. By contrast, Asp(L)60 and Glu(L)106 are almost completely shielded from the electron carriers. The charges of the Arg(H)33−Asp(H)36 ion pair and

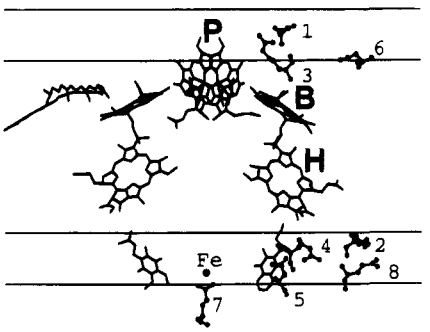

Figure 4. Ionizable residues with functional groups within 20 Å of the point midway between B and H in the *Rp. viridis* reaction center. The viewpoint and the horizontal lines indicating alternative boundaries of the nonpolar region of the membrane are as in Figure 2. The ionizable residues are 1, Asp(L)155; 2, Arg(L)103; 3. Arg(L)135; 4, Arg(H)33; 5, Asp(H)36; 6, Asp(L)60; 7, Glu(M)232; and 8, Glu(L)106.

Table 5. Effects of Ionizing Individual Amino Acid Side Chains in PDLD-Type Calculations of $\Delta\Delta G_{sol}^{pro}$ for $P^+B^-H \rightarrow P^+BH^-$ [a]

ionizable residue	distance[b] (Å)	$\Delta\Delta V_{Q\mu}$ (kcal/mol)	$\Delta\Delta G_{sol}^{pro}$ (kcal/mol) membrane[d]	$\Delta\Delta G_{sol}^{pro}$ (kcal/mol) water[e]	ϵ_{eff}[c]
Asp(L)155	13.6	−11.85	−3.67 ± 0.16	−3.15 ± 0.13	3.2
Arg(L)103	14.2	−8.57	−1.25 ± 0.04	−1.05 ± 0.03	6.9
Arg(L)135	15.3	5.29	1.71 ± 0.16	1.36 ± 0.09	3.1
Arg(H)33	16.2	−4.66	−0.04 ± 0.06	−0.10 ± 0.03	> 40
Asp(H)36	16.5	5.01	0.42 ± 0.05	0.49 ± 0.04	12
Arg(H)33 and Asp(H)36	16.2, 16.5	0.36	0.39 ± 0.05	0.41 ± 0.04	0.9[f]
Asp(L)60	17.0	−5.59	−0.55 ± 0.05	0.13 ± 0.03	10
Glu(M)232	19.8	5.14	0.22 ± 0.05	0.37 ± 0.05	23
Glu(M)232 and Fe[g]	19.8, 21.7	−6.32	−0.87 ± 0.06	−0.99 ± 0.05	7.3
Glu(L)106	19.9	4.79	0.06 ± 0.05	0.12 ± 0.02	> 40

[a] Rotatable H atoms were equilibrated with all residues neutral, and the protein was trimmed to a radius of 24 Å about a point midway between B and H. $\Delta\Delta G_{sol}^{pro}$ is the difference between the calculated value of ΔG_{sol}^{pro} for the reaction $P^+B^-H \rightarrow P^+BH^-$ when the indicated amino acid is ionized and when this residue is neutral; $\Delta\Delta V_{Q\mu}$ is the difference between the corresponding values of $\Delta V_{Q\mu}$. All other ionizable residues were in their neutral states. The uncertainties in $\Delta\Delta G_{sol}^{pro}$ are standard errors of the means of results for 10 different grids; these are smaller than the uncertainties in ΔG_{sol}^{pro} because the same set of grids was used for both the ionized and neutral states of the amino acids. [b] Distance of the ionizable functional group from the center of the trimmed protein. [c] $\Delta\Delta V_{Q\mu}/\Delta\Delta G_{sol}^{pro}$ in the model that includes a membrane.[d] [d] The membrane model included a 25-Å nonpolar region with $K = 0.119$; volume elements in internal cavities of the protein were given $K = 0.256$. [e] All solvent grid points treated as water ($K = 0.256$). [f] For the ion pair. [g] Charge = −1.0 on Glu(M)232 and +2.0 on non-heme Fe.

Table 6. Effects of Ionizing Individual Amino Acid Side Chains on FEP/MD Calculations of $\Delta\Delta G_{sol}^{pro}$ for $P^+B^-H \rightarrow P^+BH^-$ [a]

ionizable residue	$\Delta\Delta V_{Q\mu}$ (kcal/mol)	$\Delta\Delta G_{sol}^{pro}$ (kcal/mol) X-ray water only	$\Delta\Delta G_{sol}^{pro}$ (kcal/mol) with solvent	ϵ_{eff} [b]
Asp(L)60	−5.6	−7.0	−1.2	4.7
Arg (L)103	−8.6	−12.0	−0.5	17

[a] The protein system contained the water molecules seen in the X-ray structure, with or without mobile solvent water. The crystallographic water molecules were treated explicitly; the solvent waters were represented by PDLD induced dipoles. The radius of the explicit protein was 30 Å. $\Delta\Delta G_{sol}^{pro}$ is the difference between the calculated value of ΔG_{sol}^{pro} for the reaction $P^+B^-H \rightarrow P^+BH^-$ when the indicated amino acid is ionized and when this residue is neutral; $\Delta\Delta V_{Q\mu}$ is the difference between the corresponding values of $\Delta V_{Q\mu}$. All other ionizable residues were in their neutral states. [b] $\Delta\Delta V_{Q\mu}/\Delta\Delta G_{sol}^{pro}$ in the model with solvent.

Glu(M)232 also are well shielded, but charging the non-heme Fe atom along with Glu(M)232 can change ΔG_{sol}^{pro} by about −1 kcal/mol. Asp(L)155, Arg(L)103, and Arg(L)135 are potentially of special interest because they are conserved in reaction centers from a variety of bacterial species.[18] However, calculations that consider the local environments of these residues have suggested that Asp(L)155 and Arg(L)135 may not be ionized at physiological pH.[3b]

The ratio $\Delta\Delta V_{Q\mu}/\Delta\Delta G_{sol}^{pro}$ provides a screening factor, or effective dielectric constant (ϵ_{eff}), for the interactions of the electron carriers with the ionizable amino acids. For the relatively strong interactions of B and H with the ionizable groups of Asp(L)155 and Arg(L)135, ϵ_{eff} is on the order of 3 (see Table 5). A screening factor in the range of 7 is obtained for the interactions with Arg(L)103, while the screening factors for Arg(H)33 and Glu(L)106 are greater than 40. Most of the more distant ionizable residues, which resemble Glu(L)106 in being exposed to the solvent or to polar regions of the membrane, probably are sufficiently well shielded from the electron carriers so that they have little effect on the energy difference between P^+B^-H and P^+BH^-. FEP calculations (Table 6), which allow the protein structure to relax in response to changes in the charge of the ionizable group, generally give screening factors somewhat larger than those obtained in PDLD-type calculations. Much less shielding is obtained in calculations that include only the water molecules seen in the X-ray structure, which is the approximation used by Marchi et al.[4] (see Table 6).

Energetics of Charge Separation. Taken together, the PDLD-type calculations collected in Tables 1, 2, and 5 suggest that ΔG_{sol}^{pro} for the reaction $P^+B^-H \rightarrow P^+BH^-$ is approximately −5 kcal/mol, with an error range of several kilocalories per mole resulting mainly from uncertainty in the ionization states of Asp(L)155 and Arg(L)135. Combining this value with ΔV_{QQ} and ΔE^{gas} gives $\Delta G_{23}^{\circ} \approx -3$ kcal/mol. The FEP/MD values of ΔG_{sol}^{pro} and ΔE^{gas} lead to $\Delta G_{23}^{\circ} \approx +1$ kcal/mol. These values have estimated uncertainties on the order of ±3 kcal/mol. The position of P^+B^-H relative to the ground-state PBH can be obtained by subtracting ΔG_{23}° from ΔG_{03}°, the change in free energy in the overall charge-separation process $PH \rightarrow P^+H^-$. We now turn to a calculation of ΔG_{03}°.

Table 7 shows the results of PDLD calculations of ΔG_{sol}^{pro} and ΔG_{sol}^{ref} for $PH \rightarrow P^+H^-$. ΔG_{sol}^{pro} is calculated to be −36.1 kcal/mol when the protein's potentially ionizable groups are taken to be neutral, and −48.0 when all these groups are ionized. The treatment of the corresponding reference reaction for electron transfer from P to H is necessarily slightly different than that described above for the charge-shift process $P^+B^-H \rightarrow P^+BH^-$ because P cannot be removed from the reaction center

Table 7. ΔG_{sol}^{pro} for the Charge-Separation Reaction $PH \rightarrow P^+H^-$ and ΔG_{sol} for the Reference Redox Half-Reactions $P \rightarrow P^+$ and $H \rightarrow H^-$ in *Rp. viridis* Reaction Centers[a]

system[b]	$\Delta V_{Q\mu}$	ΔV_{ind}	$\Delta V_{H_2O/memb}$ [c]	ΔV_{ions}	ΔV_{bulk}	ΔG_{sol}^{pro} or ΔG_{sol}
$PH \rightarrow P^+H^-$						
ionized	−24.7	−8.0	−0.3	−12.0	−3.1	−48.0 ± 0.7[d]
neutral	−12.5	−19.1	−5.5	0.3	0.7	−36.1 ± 0.7[d]
$P \rightarrow P^+$						
ionized	3.7	−6.0	−1.2	−25.2	−6.4	−35.1 ± 0.8[e]
neutral	−4.8	−13.2	−5.8	−2.7	−2.5	−28.9 ± 0.6[e]
$H \rightarrow H^-$						
ionized	−28.3	−4.7	1.3	10.2	−6.9	−28.4 ± 0.5[e]
neutral	−7.7	−8.6	−3.1	−0.3	−3.1	−22.9 ± 0.3[e]

[a] Energies are given in kilocalories per mole and are averages of results for 10 different grids. The uncertainties given are standard errors of the means. The sum of ΔG_{sol} for $P \rightarrow P^+$ and $H \rightarrow H^-$ is ΔG_{sol}^{ref} for the complete reaction $PH \rightarrow P^+H^-$. [b] The model included all crystallographic atoms within 32 Å of either the center of P or the center of H. (The same model was used for both half-reactions and the complete reaction.) A polarizability coefficient of 0.119 was used in the 25-Å nonpolar region of the membrane and in internal cavities of the protein. The ionization states assigned to the ionizable residues were as indicated. The electrolyte charges in the water region were allowed to redistribute in response to oxidation of P or reduction of H in the reference redox reactions, but not in the charge-separation reaction; no ions were added to or removed from the system in either case. [c] $\Delta V_{H_2O} + \Delta V_{memb}$. [d] ΔG_{sol}^{pro} for the complete reaction. [e] ΔG_{sol} for the half-reaction.

for a redox titration in solution. However, P and H both can be titrated in *Rp. viridis* reaction centers, and the solvation energies can be calculated for the individual oxidation and reduction reactions in the protein. As in the charge-shift reaction, $\Delta V_{Q\mu}$ and the other individual terms that contribute to the energies vary with the size of the model and with the choice of the center of the system. The total solvation energies for the reference reactions become relatively insensitive to these details once the system is sufficiently large but, like ΔG_{sol}^{pro}, depend on the treatment of the ionizable residues. ΔG_{sol}^{ref} is found to be −51.8 kcal/mol when the ionizable groups are taken to be neutral (−28.9 kcal/mol for oxidation of P and −35.1 for reduction of H), and −63.5 kcal/mol when they are ionized (−22.9 for P and −28.4 for H). The experimentally measured value of $\mathcal{F}[E_m^H - E_m^P]$, where E_m^H and E_m^P are the midpoint potentials of the P^+/P and H/H^- couples, is approximately −25.8 kcal/mol (see ref 3b for discussion). Using the expression $\Delta E^{gas} = -\mathcal{F}[E_m^H - E_m^P] - \Delta G_{sol}^{ref}$, we thus obtain two estimates of ΔE^{gas} for the charge-separation reaction: 77.6 kcal/mol (51.8 + 25.8) from the calculations on the neutral model and 89.3 kcal/mol (63.5 + 25.8) from the calculations on the fully ionized system.

The two PDLD estimates of ΔE^{gas} can be compared with the results of INDO/S quantum calculations reported by Thompson and Zerner. Thompson and Zerner[6b] calculated a vacuum energy (ΔE^{INDO}) of 56.4 kcal/mol for $PH \rightarrow P^+H^-$ in a model that included the four BChl and two BPh molecules and the imidazole axial ligands of the BChls. ΔE^{INDO} includes the change in vacuum interactions between P and H, which we have treated separately as ΔV_{QQ}. With the atomic charges that we use, this term amounts to −19.0 kcal/mol (Table 8). Interactions with the imidazoles and the other pigments ($\Delta V_{ligands}$) contribute about −8.9 kcal/mol to the electrostatic energy of transferring an electron from P to H, and probably make a similar contribution in the quantum calculations because the resonance and inductive interactions of these components with P and H are relatively weak. In our treatment, the imidazoles and other pigments are viewed as part of the protein and enter into ΔG_{sol}^{pro} rather than ΔE^{gas}. The INDO/S vacuum energy is therefore equivalent to a ΔE^{gas} of approximately 56.4 + 19.0 + 8.9 = 84.3 kcal/mol, which is similar to the PDLD values.

Table 8. PDLD Calculations of ΔG° for $PH \rightarrow P^+H^-$ (ΔG_{03}°) and $P^*H \rightarrow P^+H^-$ (ΔG_{13}°) in *Rp. viridis* Reaction Centers[a]

ionizable residue	ΔE^{gas} [b]	ΔG_{sol}^{pro} [c]	ΔV_{QQ}	ΔG_{03}°	ΔG_{13}° [d]
ionized	89.3	−48.0	−19.0	22.3	−6.7
neutral	77.6	−36.1	−19.0	22.5	−6.5

[a] Energies are given in kilocalories per mole. The models were as in Table 7. [b] For $PH \rightarrow P^+H^-$ (see text). [c] From Table 7. [d] Calculated by subtracting the 0−0 excitation energy of P (ΔG_{01}° = 29.0 kcal/mol) from ΔG_{03}°.

Whereas the calculated values of ΔE^{gas} for the charge-separation reaction depend on the assumptions made concerning the ionizable residues, the actual value of ΔE^{gas} should be independent of the ionization state of the protein as long as the structures of P and H do not change significantly when the ionizable residues are charged. A more detailed analysis of the ionization states of the numerous residues that interact electrostatically with P^+ and H^- would be needed in order to refine the estimates of ΔE^{gas} obtained by the two limiting PDLD treatments of the ionizable groups.[20] However, such a refinement is not necessary for the present purposes. Because the charges of the ionizable groups have similar effects on the calculated values of ΔG_{sol}^{pro} and ΔG_{sol}^{ref} (see Table 7), the final value of ΔG_{03}° for the charge-separation reaction is almost independent of the charges assigned to the ionizable groups as long as the the same treatment is used for both ΔG_{sol}^{pro} and ΔG_{sol}^{ref}. The two limiting treatments of the ionizable groups both put P^+H^- in the range of 22−23 kcal/mol above the ground state, or 6−7 kcal/mol below P*H (Table 8). These results agree well with experimental studies of *Rhodobacter sphaeroides* reaction centers, which place relaxed forms of the P^+BH^- radical pair about 6 kcal/mol below P*.[5] We have shown previously[3b] that the calculated free energy of P^+H^- is insensitive to a variety of other details of the computer model, such as the size of the protein region that is treated microscopically. Combining the calculated or measured free energy of P^+H^- with the calculated ΔG_{23}° of 3 kcal/mol between P^+B^-H and P^+BH^- puts P^+B^-H below P* by 3 kcal/mol with an error range of approximately ±3 kcal/mol.

Reorganization Energies. Spectroscopic studies have suggested that P^+H^- undergoes a series of relaxations from earlier, more energetic vibrational or conformational levels on time scales of 10^{-13} to 10^{-9} s after the radical pair is created from P*.[5a,d,e,17c] The estimates of ΔG° for $PH \rightarrow P^+H^-$ and $P^+B^-H \rightarrow P^+BH^-$ obtained in the present work pertain to model systems that can relax extensively in response to the electron-transfer reaction. In the FEP/MD simulations both the protein and the solvent are free to relax; in the PDLD-type calculations, the polarizabilities are parametrized for systems in which the surrounding water relaxes fully (see the Appendix) although the protein retains the original crystal structure. The free energies calculated by the PDLD approach probably are close to those that would be found after structural relaxation of the protein, because increased induced dipoles in the water and membrane tend to compensate for underestimates of the reorientation of permanent dipoles in the protein.[9d]

The FEP/MD simulations provide estimates of the reorganization energies of the charge-separation reactions. Figure 5 shows calculated free energy surfaces of the reactant and product states for the reaction $P^+B^-H \rightarrow P^+BH^-$ with various treatments of the solvent and the ionizable amino acid side chains. With the models that included a membrane and mobile water (Figure 5A,C), the reorganization energy was calculated to be in the range of 10−15 kcal/mol, depending on the charges assigned to the ionizable residues. Similar calculations for the reaction $P^*BH \rightarrow P^+B^-H$ gave a reorganization energy of about 7 kcal/mol (not shown). These values are larger than the values of 5 kcal/mol for $P^+B^-H \rightarrow P^+BH^-$ and 4 kcal/mol for $P^*BH \rightarrow P^+B^-H$ obtained in previous, less extensive calculations on *Rb. sphaeroides* reaction centers,[3a] and seem larger than expected for reaction kinetics that are observed to be nearly independent of temperature. The calculated reorganization energy for $P^+B^-H \rightarrow P^+BH^-$ decreased to about 5 kcal/mol if the atomic charges of the noncrystallographic solvent molecules were replaced by induced dipoles on the oxygen atoms (Figure 5E). This treatment models a system in which the positions of the solvent atoms are frozen and the dielectric responses of the solvent to the electron-transfer reaction reflect only electronic polarizability. Models that omitted the mobile solvent (Figure 5B,D) also gave reorganization energies of approximately 5 kcal/mol for $P^+B^-H \rightarrow P^+BH^-$. However, the significance of the calculated reorganization energies is not entirely clear because the free energy functions are not competely parabolic, the curvatures of the functions may be different for the reactant and product states (particularly for the $P^*BH \rightarrow P^+B^-H$ charge-separation reaction), and only limited regions the free energy surfaces are well determined. In addition, it is possible that the FEP/umbrella sampling procedure forces the system to undergo a more extensive relaxation than occurs during the actual charge-separation process.

Although treating the noncrystallographic waters as uncharged and weakly polarizable decreased the calculated reorganization energy significantly for the reaction $P^+B^-H \rightarrow P^+BH^-$, it had little effect on the calculated ΔG° (compare parts E and A of Figure 5). The comparatively weak dependence of ΔG_{23}° on the details of the treatment of the solvent is in accord with the PDLD and FEP/MD results discussed above. Thus, although questions remain about what value of the time-dependent reorganization energy is most relevant to the electron-transfer kinetics, the relevant value of ΔG_{23}° appears to be well determined.

We also carried out one set of PDLD-type calculations in which the electrolyte charges and slowly-relaxing induced dipoles were frozen in configurations set by the state of the system prior to charge separation (see the Methods). With the ionizable groups neutral, ΔG_{sol}^{pro} was about 2.2 kcal/mol more positive in the frozen system than in the relaxed system. If the ionizable residues were ionized, the frozen system gave values of ΔG_{sol}^{pro} that were about 5.6 kcal/mol more negative than those obtained for the relaxed system (Table 3). The sensitivity of the PDLD ΔG_{sol}^{pro} value to the charges of the ionizable residues thus is considerably larger if the low-frequency fluctuations of dipoles are frozen. Note, however, that the frozen model will underestimate the screening of $\Delta V_{Q\mu}$ because it corresponds to the limit of zero nuclear reorganization energy. Some relaxation is expected in any polar system.

Discussion

The results presented above emphasize the importance of the solvent in the primary electron-transfer steps in bacterial reaction

(20) (a) Several considerations[20b,c] suggest that the true value of ΔE^{gas} is likely to be closer to the value calculated with the nonionized model (77.6 kcal/mol) than to the higher value obtained with the ionized model. (b) The INDO/S quantum calculations[6b] overestimate the energy of the excited state P* by about 4 kcal/mol, implying that ΔE^{gas} for $PH \rightarrow P^+H^-$ probably is lower than the calculated value of 84.3 kcal/mol. However, this error could be partly offset by inductive effects that we have neglected in relating the INDO/S vacuum energy to ΔE^{gas}. (c) In work currently in progress, Asp(L)155 and several other aspartate residues in *Rb. sphaeroides* reaction centers have been replaced by lysines by site-directed mutagenesis. The observed effects on the E_m of P^+/P are smaller than predicted by PDLD calculations in which the charges on the other ionizable residues are held constant (S. Rongey, M. Okamura, V. Nagarajan, R. Alden, and W. Parson, unpublished results). The effective screening of charged groups near the surface of the protein evidently is greater than the PDLD calculations would suggest.

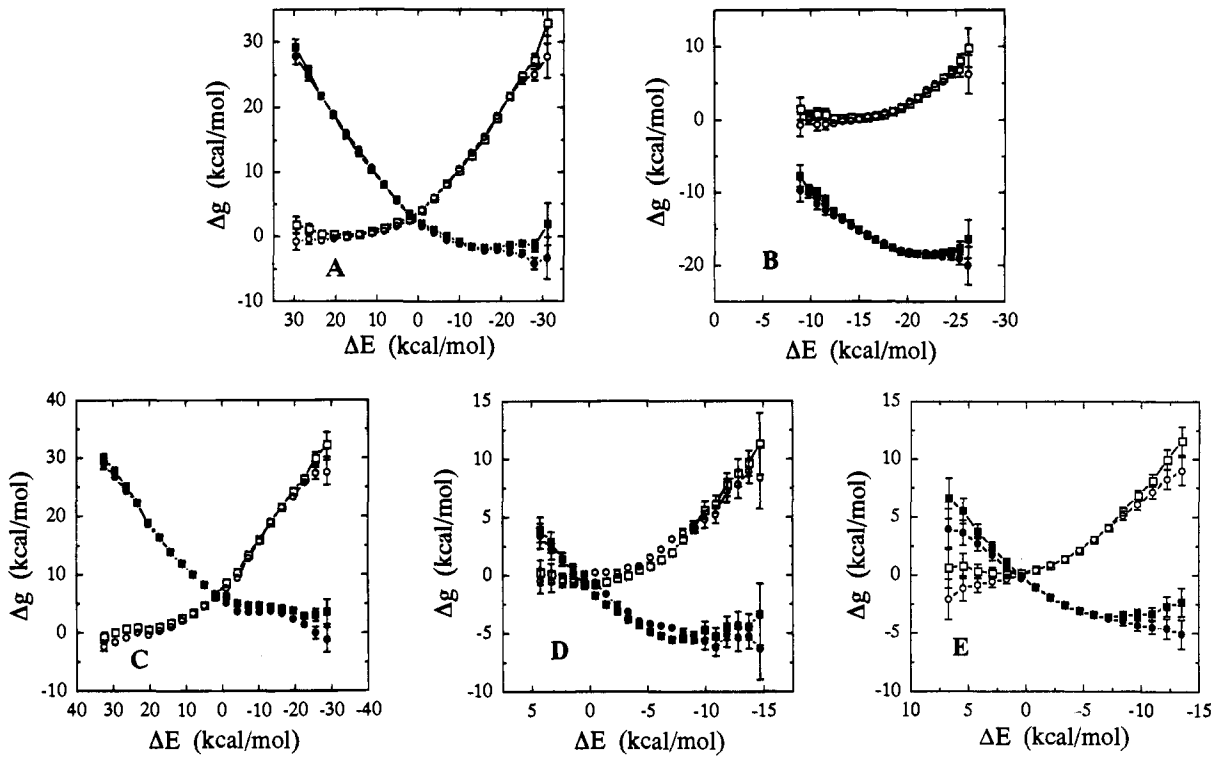

Figure 5. Free energy surfaces for $P^+B^-H \rightarrow P^+BH^-$ in FEP/MD simulations: (*A*) with membrane and solvent, ionizable side chains ionized; (B) without membrane or solvent (X-ray waters only), ionizable side chains ionized; (C) with membrane and solvent, ionizable side chains neutral; (D) without membrane or solvent, ionizable side chains neutral; (E) with membrane and solvent, but with the atomic charges of the noncrystallographic water molecules omitted and replaced by induced dipoles, ionizable side chains ionized. In (A) and (C), the atomic charges of the noncrystallographic waters were treated explicitly; in (E), the O atoms of these waters were given an atomic polarizability of 1.3 Å^3 corresponding to $\epsilon \approx 2$. Other conditions were as in Table 4. The abscissas give the energy differences between P^+BH^- and P^+B^-H, including ΔE^{gas} and ΔV_{QQ}. These energies, which fluctuate during the molecular-dynamics trajectories, provide the most useful measure of the reaction coordinates.[15] The ordinates give the relative free energies of P^+BH^- (filled symbols) and P^+B^-H (open symbols) in each model. The two curves for each state (circles and squares) were obtained by evaluating the set of six MD trajectories in opposite orders, so that the system evolved either from P^+B^-H to P^+BH^- or from P^+BH^- to P^+B^-H. These curves should be equivalent if the trajectories are sufficiently long. The error bars indicate the relative sampling errors of the points, which are proportional to $n^{-1/2}$ where n is the total number of occurrences of the particular value of ΔE indicated on the abscissa. Repeating the calculations with a range of models gives a more realistic estimate of the true uncertainties in the calculated free energy functions.

centers. In addition to increasing the solvation of the radicals P^+, B^-, and H^-, the solvent that surrounds the protein and fills its cavities will shield the electron carriers from the field of ionized amino acid side chains. As a result of this shielding, most of the ionized groups probably do not contribute significantly to the free energy difference between the relaxed P^+B^-H and P^+BH^- states. A large attenuation of the effects of the ionized residues is obtained even in models that include a membrane with a low polarizability in the region of the electron carriers. By contrast, calculations that omit the membrane and solvent give results that are unrealistically sensitive to distant charges.

Because the mobile water, lipids, and ions that surround the reaction center are not resolved in the crystal structure, it is necessary to add these molecules to the computer model. The nature of the material that fills the cavities of the protein is not entirely clear.[21] Fortunately, the calculated value of ΔG_{sol}^{pro} depends only weakly on whether the cavities in the nonpolar region of the protein are empty or are occupied by water or lipids (Table 2). It also is insensitive to whether the protein in the model is embedded in water or a membrane, and in the latter case, on the thickness and polarizability assigned to the membrane's hydrophobic region (Table 1).

Much of the uncertainty in our estimate of ΔG_{sol}^{pro} lies in the interactions of B and H with a small number of ionizable amino acid residues. The interactions with Asp(L)155, Arg(L)103, and Arg(L)135 stand out in this regard (Table 7). Most of the more distant ionized goups are likely to be sufficiently well solvated so that they have only small effects on the energies of the radical-pair states. Whether Asp(L)155, Arg(L)103, and Arg(L)135 actually are ionized at physiological pH is uncertain.[3b] To refine the computer models that we have used, it will be necessary to establish the protonation state of each of these residues, taking into account interactions with all the other ionizable groups, the membrane, and the solvent. We currently are attempting to probe the roles of the potentially important ionizable residues experimentally by examining the effects of mutations on the electron-transfer kinetics and the redox potentials of the electron carriers.[20c]

When the solvation of the electron carriers and the charged amino acids by the membrane and water surrounding the protein are taken into account, the free energy difference between relaxed forms of P^+B^-H and P^+BH^- is calculated to be on the order of 3 kcal/mol. Variations in the treatments of the membrane and solvent, the ionizable amino acid side chains, and the non-heme Fe can shift the calculated value up or down by several kilocalories per mole. The calculated values of $\Delta G_{23}°$

(21) (a) In principle, the number of water molecules present in a given cavity can be established by considering the free energy of transfer from aqueous solution. By searching for positions where water molecules could form three hydrogen bonds to the protein or to other bound waters, Beroza et al.[21b] have identified about twice as many potential binding sites in the *Rp. viridis* reaction center as the number of waters resolved in the X-ray structure. Beroza et al. note that additional waters are likely to occupy internal channels and cavities that their search procedure did not consider. More rigorous searches would require FEP calculations of the free energy of introducing water in a cavity of the protein, relative to the free energy of forming bulk water. (b) Beroza, P.; Fredkin, D. R.; Okamura, M. Y.; Feher, G. In *The Photosynthetic Reaction Center II*; Breton, J., Verméglio, A., Eds.; Plenum Press: New York, 1992; pp 363–374.

put P^+B^-H slightly below P*, which appears to be consistent with the formation of P^+B^-H as an intermediate in the charge-separation reaction. However, the uncertainties in the calculations leave open the possibilty that P^+B^-H lies above P* by several kilocalories per mole, which would be too large an energy gap to surmount rapidly by thermal fluctuations. In this situation, electron transfer from P* to H would have to rely on superexchange, particularly at low temperatures. If the energy gap between P* and P^+B^-H were larger than several kilocalories per mole, the superexchange mechanism also would have difficulty accounting for the speed of the reaction, because the interaction matrix element that mixes these states then would have to be significantly larger than current theoretical estimates.[3d,22]

The results shown in Figure 3 indicate that the disagreement between our conclusions and those of Marchi et al.[4] does not result from our having truncated the protein model too abruptly, as Marchi et al. suggested. Once the explicit model extends beyond about 20 Å from the electron carriers, further increases in size have relatively little effect on the calculated value of ΔG_{sol}^{pro}. Nor does the problem seem to lie in other detailed features of the computer models used because, as long as the medium around the protein is included, variations in these details also cause only minor changes in our results. Instead, the disagreement appears to hinge primarily on our very different treatments of dielectric effects.

Marchi et al.[4] started with vacuum INDO/S energies that Thompson and Zerner[6b] had calculated for the reactions $P^* \rightarrow P^+B^-$ and $P^* \rightarrow P^+H^-$. As was discussed above, these energies (ΔE^{INDO}, or $\Delta\epsilon^{(0)}$ in the notation used by Marchi et al.) include interactions among all four BChls and both BPhs of the reaction center and also the interactions with the axial ligands of the BChls. Marchi et al. evaluated the vacuum electrostatic interactions among the pigments and histidines (ΔV_{pigm}, or ν in their notation) and subtracted them from the total vacuum electrostatic energy (ΔV_{elec} or $\Delta\epsilon$). Rather than evaluating induced dipoles microscopically as we have done, they scaled $\Delta V_{elec} - \Delta V_{pigm}$ by an adjustable factor ($1/\epsilon$) that was intended to represent dielectric effects. Their final expression for the free energy change was

$$\Delta G^\circ = \Delta E^{INDO} + (\Delta V_{elec} - \Delta V_{pigm})/\epsilon \qquad (16)$$

Marchi et al. adjusted ϵ to make the calculated ΔG° for $P^*H \rightarrow P^+H^-$ match the experimentally measured free energy change. They regarded the necessary value of ϵ (1.9) as physically reasonable because it was similar to the high-frequency dielectric constant of most dense liquids (ϵ_∞).

If all of the ionizable groups of the protein are considered to be charged, the magnitude of the term $\Delta V_{elec} - \Delta V_{pigm}$ is considerably smaller for the reaction $P^*B \rightarrow P^+B^-$ than for $P^*H \rightarrow P^+H^-$. Marchi et al.[4] obtained a value of −49.0 kcal/mol for the formation of P^+H^- and −9.1 kcal/mol for P^+B^-. The quantum term ΔE^{INDO}, on the other hand, was reported to be similar for the two reactions.[6b] Applying eq 16 to the P^+B^- radical pair therefore left this state far above P* in energy.

Neglecting ΔV_{ions} (which Marchi et al. did not consider), the total vacuum electrostatic energy ΔV_{elec} of eq 16 is equivalent to $\Delta V_{QQ} + \Delta V_{Q\mu}$ in our notation.[23] ΔV_{pigm} can be written as $\Delta V_{QQ} + \Delta V_{ligands}$, where $\Delta V_{ligands}$ represents the vacuum interactions of the electron carriers with the other pigments and the imidazole axial ligands of the BChls. By making these substitutions and incorporating the relationship $\Delta E^{INDO} \approx \Delta E^{gas} + \Delta V_{QQ} + \Delta V_{ligands}$ (see above), eq 16 can be rewritten as

$$\Delta G^\circ = \Delta E^{gas} + \Delta V_{QQ} + \Delta V_{ligands} + (\Delta V_{Q\mu} - \Delta V_{ligands})/\epsilon \qquad (17)$$

Apart from the question of whether the dielectric properties of the protein, membrane, mobile ions, and solvent can be represented realistically by a homogeneous dielectric constant, eqs 16 and 17 are fundamentally incorrect.[25b] As has been pointed out elsewhere,[3c,e] these expressions do not incorporate the energy that the system would have if the electron carriers were removed from the protein and separated to infinite distance in a medium with dielectric constant ϵ. Moving the pigments apart would reduce ΔV_{QQ}, $\Delta V_{Q\mu}$, and $\Delta V_{ligands}$ all to zero, making ΔG° incorrectly equal to ΔE^{gas} according to eq 17. In addition, eqs 16 and 17 do not consider the screening of ΔV_{QQ} and $\Delta V_{ligands}$ by the dielectric medium when the electron carriers are in their actual positions. A correct expression for the energetics of charge separation in a medium with a homogenous dielectric constant ϵ (still neglecting mobile ions) is[3e]

$$\Delta G^\circ \approx \Delta E^{gas} + \Delta G_{sol}^{\epsilon,\infty} + (\Delta V_{QQ} + \Delta V_{Q\mu})/\epsilon \qquad (18)$$

where $\Delta G_{sol}^{\epsilon,\infty}$ is the difference between the solvation energies of the products and reactants when the electron carriers are at infinite separation in the same solvent.

Methods of calculating the "self-energy" term $\Delta G_{sol}^{\epsilon,\infty}$ in eq 18 have been discussed elsewhere.[3e,24] For the reaction $PH \rightarrow P^+H^-$, $\Delta G_{sol}^{\epsilon,\infty}$ is given approximately by (−76.7 kcal/mol)(1 − $1/\epsilon$). ΔV_{QQ} for this reaction is −19.0 kcal/mol, and with the neutral structural model described in Table 7, $\Delta V_{Q\mu}$ is −12.5 kcal/mol (see Tables 7 and 8). If we use $\Delta E^{gas} \approx 83$ kcal/mol (the average of the two PDLD estimates described above), then $\Delta G^\circ \approx 6.3 + 45.2/\epsilon$ kcal/mol. This expression reproduces the experimental estimate of ΔG° for the formation of P^+H^- from PH (23 kcal/mol) when $\epsilon = 2.7$. Using the quantum estimate of 84.3 kcal/mol for ΔE^{gas} gives very similar results. If the

(22) (a) Parson, W. W.; Creighton, S.; Warshel, A. In *Primary Processes in Photobiology*; Kobayashi, T., Ed.; Springer-Verlag: Berlin, 1987; pp 43−51. (b) Warshel, A.; Creighton, S.; Parson, W. W. *J. Phys. Chem.* **1988**, *92*, 2696−2701. (c) Scherer, P. O. J.; Fischer, S. F. *Chem. Phys.* **1987**, *115*, 151−158. (d) Scherer, P. O. J.; Fischer, S. F. *Chem. Phys.* **1989**, *131*, 115−127. (e) Scherer, P. O. J.; Fischer, S. F. *J. Phys. Chem.* **1989**, *93*, 1633−1637. (f) Plato, M.; Winscom, C. J. In *The Photosynthetic Reaction Center*; Breton, J., Verméglio, A., Eds.; Plenum Press: New York, 1988; pp 421−424.

(23) In the treatment described by Marchi et al.[4] ΔV_{elec} (their $\Delta\epsilon$) and ΔV_{pigm} (ν) represent averages over a molecular-dynamics trajectory, whereas in the PDLD treatment $\Delta V_{Q\mu}$, ΔV_{QQ}, and $\Delta V_{ligands}$ are calculated using the crystallographic coordinates for all atoms other than hydrogens. This difference does not affect our argument in principle, although the calculated values of the corresponding energies are expected to vary somewhat as a result of equilibration of the crystal structure by molecular dynamics or energy minimization of the polar hydrogens, and also from the use of different atomic charges. For example, we distributed the charges of P^+, B^-, or H^- over all the π atoms of the electron carrier whereas Marchi et al. concentrated the charges on the pyrrole nitrogens. When the entire protein was included in the model, and all the ionizable residues, the crystallographically resolved N-terminal amino groups and C-terminal carboxyl groups, the heme propionyl carboxyls, and the non-heme Fe were charged, we obtained $\Delta V_{Q\mu} + \Delta V_{QQ} = -62.8$ kcal/mol for the reaction $PH \rightarrow P^+H^-$, whereas Marchi et al.[4] reported $\Delta V_{elec} = -81.3$ kcal/mol.

(24) (a) $\Delta G_{sol}^{\epsilon,\infty} \approx \Delta G_{sol}^{w,\infty}(1 - 1/\epsilon)$, where $\Delta G_{sol}^{w,\infty}$ is the change in solvation energies in the electron-transfer reaction when the electron carriers are at infinite separation in water or another polar solvent.[3e] $\Delta G_{sol}^{w,\infty}$ can be calculated by the PDLD approach, and for the reaction $P + H \rightarrow P^+ + H^-$ is approximately −76.7 kcal/mol.[3e] If ΔE^{gas} is obtained by similar PDLD calculations and experimentally measured redox potentials (eq 2), the values of ΔE^{gas} and $\Delta G_{sol}^{w,\infty}$ are negatively correlated in the manner discussed above for ΔE^{gas} and $\Delta G_{sol}^{w,\infty}$. Free energies calculated by eq 18 thus are insensitive to variations in the treatment of the solvation energies. For the reaction $B^-H \rightarrow BH^-$, the sum of ΔE^{gas} and $\Delta G_{sol}^{w,\infty}$ is uniquely determined by the measured value of $\mathcal{F}[E_m^B - E_m^H]$. (b) Equation 18 is based on the generalized Born expression, which is more reliable than the reaction-field approach that Thompson and Zerner[6b] have used to incorporate the effects of a nonpolar dielectric continuum into quantum calculations.

same macroscopic treatment of dielectric effects is applied to P^+B^-, values of ϵ that position P^+H^- at the experimentally observed energy put P^+B^- between P* and P^+H^-.[3e,24b]

A simple macroscopic treatment that includes all the relevant terms thus appears to be fully consistent with the conclusions from our PDLD and FEP calculations concerning the energy of P^+B^-. The macroscopic picture is instructive because it shows, in agreement with the PDLD calculations, that a large electrostatic field from the protein is not needed in order to make the formation of P^+H^- from P*H exothermic by about the amount seen experimentally, even in a medium with a dielectric constant on the order of 2–3. However, such macroscopic models are major oversimplifications of the dielectric effects that contribute to this heterogeneous system. The stable values of ΔG_{sol}^{pro} that we obtained for models of varying sizes and charges (Figure 3 and Tables 1 and 2) could not be obtained simply by scaling $\Delta V_{QQ} + \Delta V_{Q\mu}$ by a constant factor of $1/\epsilon$.[25] Nor would a constant scaling of $\Delta V_{QQ} + \Delta V_{Q\mu}$ by $1/\epsilon_\infty$ reproduce the large, anisotropic screening of the fields of individual ionizable amino acid residues (Table 7). Many of the protein's ionizable groups are located near the surfaces of the protein on either side of the membrane and probably would not be ionized if they were not well solvated by the surrounding water. A realistic treatment of the system requires consideration of the solvent in addition to an explicit representation of the protein's permanent dipoles. Recent calculations by Gunner et al.[26] are in accord with this view. Smith and Pettit[10b] also have stressed the importance of the solvent in computer simulations of biomolecules and have reviewed the strengths and limitations of models that have been used to treat the solvent at varying levels of complexity.

As shown in the second column of Table 6, FEP calculations that omit mobile solvent drastically overestimate charge–charge interactions in the protein. These interactions evidently are screened strongly by the solvent. This conclusion is consistent with experimental observations on both the reaction center and other proteins. For example, the mutation Asp99 → Ser in subtilisin causes a shift of 0.4 pH unit in the pK_a of a histidyl side chain in the enzyme's active site, between 12 and 13 Å from the Asp carboxyl group.[27] This effect corresponds to a screening of electrostatic interactions between the His and Asp side chains by an effective dielectric constant of 50. The mutation of Glu156 to Ser gives very similar results.[27] Previous calculations using PDLD or FEP methods[9,28] or finite-difference treatments of the linearized Poisson–Boltzmann equation[10,11,29] have reproduced the large screening of charge–charge interactions in water-soluble proteins. A large screening of interactions between Arg38 and the heme is seen experimentally in cytochrome *c*, and is reproduced well in FEP calculations that include a PDLD treatment of the solvent.[28]

In reaction centers of *Rb. sphaeroides*, reduction of the quinone Q_A has relatively little effect experimentally on either the kinetics of the initial electron-transfer reaction or the apparent free energy difference between P* and P^+H^-,[30] while placing an unscreened negative charge on the quinone would increase the energy for transferring an electron from P* to H by 10.7 kcal/mol.[31a] Recent work on the effects of mutating several ionizable residues indicates that the screening of these residues from P^+ is, if anything, greater than the PDLD calculations suggest.[20c] Steffen et al.[32] have obtained estimates of the dielectric constant in the interior of the reaction center by measuring shifts in the absorption spectra of the pigments in response to the formation of P^+, Q_A^-, or the $P^+Q_A^-$ radical pair. The spectral shifts caused by the internal electric fields of P^+ and Q_A^- were compared with the Stark effects of external fields. At 1.5 K, the dielectric constants for interactions of H with P^+, Q_A^-, and $P^+Q_A^-$ were estimated to be approximately 6.8, 5.8, and 4.5, respectively. The dielectric constants at 298 K were judged to be about twice as large. These values are comparable to the screening factors that we have calculated for interactions of P^+B^- and P^+H^- with the closest ionizable residues (Tables 5 and 6). The effective dielectric constants for interactions of more widely separated charged groups would be expected to be larger than the dielectric constants obtained by Steffen et al., which pertain to local regions of the protein.[7] Steffen et al.[32] concluded also that the dielectric constant in the region of the photochemically inactive BPh (H_M) was only about half that in the region of the photochemically active BPh (H_L). Although we have not considered H_M specifically in the present work, and it appears to us that there could be alternative explanations for Steffen et al.'s observations on this point,[33] the conclusion that the local dielectric in the reaction center is strongly anisotropic is in accord with our results.

It is important to note that most of the calculations described in the present work pertain to equilibrated systems. The screening of electrostatic interactions is likely to be weaker on the short time scale of the charge-separation steps in the reaction

(25) (a) When the ionizable side chains in the structural model described in Table 7 are ionized, $\Delta V_{Q\mu}$ for the reaction PH → P^+H^- is −24.7 kcal/mol. Equation 18 (with $\Delta E^{gas} = 83$ and $\Delta V_{QQ} = -19.0$ kcal/mol) then gives $\Delta G^\circ \approx 6.3 + 33.0/\epsilon$ kcal/mol, which reproduces the experimental estimate of ΔG° (23 kcal/mol) when $\epsilon = 2.0$. This model includes all the protein atoms within 32 Å of either P or H. If the model is expanded to include the entire protein with all of the ionizable side chains and also the ionizable N- and C-terminal groups and heme propionyl carboxyls charged, $\Delta V_{Q\mu}$ becomes −43.8 kcal/mol. Equation 18 now gives $\Delta G^\circ \approx 6.3 + 13.9/\epsilon$, which requires $\epsilon = 0.8$ in order to reproduce the experimental estimate of ΔG°. If all the protein charges are neglected except for those of the imidazole axial ligands of P and B, $\Delta V_{Q\mu}$ is −8.9 kcal/mol and eq 18 gives $\Delta G^\circ \approx 6.3 + 48.8/\epsilon$, which fits the experimental ΔG° with $\epsilon = 2.9$. The fact that the necessary value of ϵ depends on $\Delta V_{Q\mu}$ and can be less than 1 does not mean that the macroscopic model should be dismissed immediately. It simply indicates that ϵ is a model-dependent, effective screening factor and should not be viewed as the actual dielectric constant for charge–charge interactions in the protein.[3e,7a] (b) Marchi et al.'s[4] finding that they could reproduce the measured ΔG° of the reaction PH → P^+H^- by using the incorrect eq 17 with a value of ϵ that seemed physically reasonable for the interior of a hydrophobic protein appears to reflect an accidental cancellation of the results of, on the one hand, omitting the terms $\Delta G_{sol}^{\epsilon,\infty}$ and $-(\Delta V_{QQ} + \Delta V_{ligands})(1 - 1/\epsilon)$ and, on the other, including a large negative $\Delta V_{Q\mu}$ from unscreened ionized residues. For $\epsilon = 2$, the missing terms in eq 17 amount to approximately −24 kcal/mol $[(\Delta G_{sol}^{w,\infty} - \Delta V_{QQ} - \Delta V_{ligands})(1 - 1/\epsilon) \approx (-76.7 + 19.0 + 8.9)/2]$. A similar cancellation does not occur in the case of the charge-shift reaction P^+B^-H → P^+BH^-, for which $\Delta G_{sol}^{w,\infty}$ is much smaller (about −12.1 kcal/mol, compared to −76.7 kcal/mol for PH → P^+H^-).[3e]

(26) Gunner, M. R.; Nicholls, A.; Honig, B. Submitted for publication.

(27) Russell, A. J.; Thomas, P. G.; Fersht, A. R. *J. Mol. Biol.* **1987**, *193*, 803–813.

(28) Cutler, R. L.; Davies, A. M.; Creighton, S.; Warshel, A.; Moore, G. R.; Smith, M.; Mauk, A. G. *Biochemistryy* **1989**, *28*, 3188–3197.

(29) (a) Bashford, D.; Karplus, M. *Biochemistry* **1990**, *29*, 10219–10225. (b) Antosiewicz, J.; McCammon, A.; Gilson, M. K. *J. Mol. Biol.* **1994**, *238*, 415–436.

(30) (a) Woodbury, N. W.; Becker, M; Middendorf, D.; Parson, W. W. *Biochemistry* **1985**, *24*, 7516–7521. (b) Woodbury, N. W.; Parson, W. W.; Gunner, M. R.; Prince, R. C.; Dutton, P. L. *Biochim. Biophys. Acta* **1986**, *851*, 6–22. (c) Martin, J.-L.; Breton, J.; Hoff, A. J.; Migus, A.; Antonetti, A. *Proc. Natl. Acad. Sci. U.S.A.* **1986**, *83*, 957–961.

(31) (a) To calculate the effect of Q_A on $\Delta V_{Q\mu}$ for the reaction PH → P^+H^-, we used the quantum-mechanical-consistent-force-field/π-electron (QCFF/PI) treatment[31b] to find the atomic charges for Q_A and Q_A^-. The calculations were based on the crystal structure of reaction centers from *Rb. sphaeroides*,[1b,c] in which Q_A is ubiquinone. (b) Warshel, A.; Lappicirella, V. A. *J. Am. Chem. Soc.* **1981**, *103*, 4664–4673.

(32) Steffen, M.; Lao, K.; Boxer, S. G. *Science* **1994**, *264*, 810–816.

(33) For example, the hydrogen bond between Glu(L)104 and the ring-V keto group of H_L could rotate the vector for the change in permanent dipole moment associated with the Q_y transition, which would alter the observed response to an oriented electric field. H_M is not hydrogen-bonded in this way. The spectroscopic band shifts also could be complictated by exciton interactions of the BPh molecules with the neighboring BChls, and by changes in the electric fields resulting from binding or dissociation of protons.

center, particularly at low temperatures. Fields from ionized groups of the protein could, therefore, influence the electron-transfer dynamics significantly under some conditions, as several researchers have suggested.[26,34]

In summary, we have shown that models with proper dielectric boundaries lead to calculated electrostatic energies that are relatively insensitive to the assumptions made concerning the solvent and the charges assigned to ionized groups of the protein. Using such models leads to good agreement with the experimentally measured energy of the relaxed P^+H^- radical pair and places P^+B^-H close to P* in energy. By contrast, treatments that neglect the self-energies of the electron carriers and do not account for the screening of the field of the ionized residues place P^+B^-H substantially above P*. The need for realistic treatments of dielectric effects in computational studies is relevant, not only to the primary charge-separation process in photosynthesis, but also to many other problems that involve electrostatic energies in macromolecules.

Acknowledgment. This work was supported by NIH Grant GM-40283 and NSF Grants DCM-86188563 and DMB-9111599. R.G.A. was funded partly by NSF Postdoctoral Fellowship in Plant Biology Grant DIR-9104322. We thank Drs. David Chandler and Marilyn Gunner for helpful discussions.

Appendix: A Simplified Treatment of Dielectric Effects in Water

In the standard PDLD treatment,[7-9] water dipoles are described by a Langevin-type function:

$$\mu_i = \hat{\xi}_i \upsilon_i \mu_{max}(\coth \chi_i - 1/\chi_i) \quad \text{(A1)}$$

$$\chi_i = \gamma \mu_{max} |\xi_i| / k_B T \quad \text{(A2)}$$

Here $\hat{\xi}_i$ is a unit vector in the direction of the field (ξ_i) at grid point i, $\mu_{max} \approx 0.35$ e·Å, γ is an adjustable parameter that usually is set ~ 1 e^{-2}·Å·kcal^{-1}·mol, and υ_i is the volume associated with point i. This expression models the average orientation of the permanent dipoles of the water molecules by the field. A linear term, $\hat{\xi}_i \upsilon_i K_i |\xi_i|$, can be included to describe the additional contribution from electronic polarizability.

Although the Langevin treatment has been used successfully in numerous applications, the approach to convergence tends to be oscillatory and to require a large number of iterations. We therefore explored using the simple linear expression

Table 9. Calculated solvation energies for charging Na^+ or Cl^- in water in the presence of another ion with the same or opposite charge[a]

test ion	2nd ion	distance[b] (Å)	$\Delta V_{Q\mu}$ (kcal/mol)	ΔV_{H_2O} (kcal/mol)	ΔV_{bulk} (kcal/mol)	ΔG_{sol} (kcal/mol)
Cl^-	none			−71.0	−8.4	−79.4 ± 1.5
	Na^+	8	−41.5	−47.0	8.5	−80.1 ± 1.0
		10	−33.2	−55.1	8.5	−79.8 ± 1.5
		12	−27.7	−58.9	8.5	−78.0 ± 1.3
		14	−23.7	−63.0	8.5	−78.2 ± 1.6
	Cl^-	8	41.5	−98.3	−25.4	−82.1 ± 0.9
		10	33.2	−89.9	−25.3	−82.0 ± 1.5
		12	27.7	−82.8	−25.3	−80.4 ± 0.9
		14	23.7	−79.0	−25.2	−80.6 ± 1.5
Na^+	none			−94.5	−8.4	−102.9 ± 4.2
	Cl^-	8	−41.5	−70.9	6.6	−105.8 ± 2.1
		10	−33.2	−75.4	6.6	−102.1 ± 1.5
		12	−27.7	−82.3	6.6	−103.4 ± 2.1
		14	−23.7	−82.2	6.6	−99.3 ± 1.6
	Na^+	8	41.5	−116.2	−25.4	−100.0 ± 4.2
		10	33.2	−106.7	−25.4	−98.9 ± 3.6
		12	27.7	−100.2	−25.3	−97.9 ± 2.7
		14	23.7	−97.1	−25.3	−98.7 ± 3.8

[a] The Cl^- and Na^+ ions were assigned solvent exclusion radii of 2.5 and 2.1 Å, respectively. $\Delta V_{Q\mu}$ is the energy of interaction between the two ions, calculated with Coulomb's law with $\epsilon = 1$. ΔG_{sol} is the total change in solvation energy for charging the test ion, including $\Delta V_{Q\mu}$, ΔV_{H_2O}, and ΔV_{bulk}. The solvent grid had a radius of 20 Å, a spacing of 2.0 Å in the region within 14 Å of the center and 3.0 Å outside this region, and a polarizability coefficient (K) of 0.256. The uncertainties in ΔG_{sol} are standard errors of the means of results for 10 different grids centered at random points up to 2 Å from the point midway between the two ions, or from the test ion if the system had only one ion. [b] Distance between the two ions.

$$\mu_i = K \upsilon_i \xi_i \quad \text{(A3)}$$

We optimized the value of K by calculating the solvation energies of monovalent anions and cations and by evaluating the apparent dielectric constant for interactions of ions with the same or opposite charges. We also tried including a quadratic term ($\lambda \upsilon_i \hat{\xi}_i |\xi|^2$ with $\lambda < 0$) to give the dependence on $|\xi_i|$ an adjustable curvature, but this proved unnecessary.

Table 9 gives the calculated solvation energies for charging Cl^- or Na^+ in water in the presence of another ion with either the same or opposite charge. The calculations include the terms $\Delta V_{Q\mu}$, ΔV_{H_2O}, and ΔV_{bulk}, but no additional electrolytes (ΔV_{ions}); the induced dipoles in the solvent grid were calculated by eq A3 with $K = 0.256$. Note that, although the energy of the unscreened interaction between the two ions ($\Delta V_{Q\mu}$) varies over a range of 83 kcal/mol depending on the charge of the second ion and on the distance between the ions, the values of ΔG_{sol} for charging an ion of a given size are almost constant and are close to the value obtained in the absence of the second ion. This indicates that the treatment successfully models the effects of a solvent with a large dielectric constant. In addition, the calculated magnitudes of ΔG_{sol} are close to the experimental electrostatic solvation free energies of Cl^- and Na^+ in water (−77 ± 5 and −100 ± 5 kcal/mol, respectively[9a,35]). The calculations usually converged within 7−10 iterations, which is about half the number that the Langevin treatment requires.

JA944105B

(34) Middendorf, T. R.; Mazzola, L. T.; Lao, K., Steffen, M. A.; Boxer, S. G. *Biochim. Biophys. Acta* **1993**, *1143*, 223−234.
(35) (a) Noyes, R. M. *J. Am. Chem. Soc.* **1962**, *84*, 513−522. (b) Rossinsky, D. R. *Chem. Rev.* **1965**, *65*, 467−490. (c) Miller, W. A.; Watts, D. W. *J. Am. Chem. Soc.* **1967**, *89*, 6051−6056. (d) Friedman, H. L.; Krishann, C. V. In *Water- A Comprehensive Treatise*; Franks, F., Ed.; Plenum Press: New York, 1973; Vol. 3, pp 1−118.